JEM

Article

Cbfβ2 controls differentiation of and confers homing capacity to prethymic progenitors

Mari Tenno,[1]* Satoshi Kojo,[1]* Divine-Fondzenyuy Lawir,[4] Isabell Hess,[4] Katsuyuki Shiroguchi,[2,5,6] Takashi Ebihara,[1] Takaho A. Endo,[3] Sawako Muroi,[1] Rumi Satoh,[7] Hiroshi Kawamoto,[7] Thomas Boehm,[4] and Ichiro Taniuchi[1]

[1]Laboratory for Transcriptional Regulation, [2]Laboratory for Immunogenetics, and [3]Laboratory for Integrative Genomics, RIKEN Center for Integrative Medical Sciences, Yokohama, Kanagawa, Japan
[4]Department of Developmental Immunology, Max-Planck Institute of Immunobiology and Epigenetics, Freiburg, Germany
[5]Laboratory for Integrative Omics, RIKEN Quantitative Biology Center, Osaka, Japan
[6]Precursory Research for Embryonic Science and Technology (PRESTO), Japan Science and Technology Agency, Saitama, Japan
[7]Laboratory for Lymphocyte Development, RIKEN Center for Allergy and Immunology, Yokohama, Japan

Multipotent hematopoietic progenitors must acquire thymus-homing capacity to initiate T lymphocyte development. Despite its importance, the transcriptional program underlying this process remains elusive. Cbfβ forms transcription factor complexes with Runx proteins, and here we show that Cbfβ2, encoded by an RNA splice variant of the *Cbfb* gene, is essential for extrathymic differentiation of T cell progenitors. Furthermore, Cbfβ2 endows extrathymic progenitors with thymus-homing capacity by inducing expression of the principal thymus-homing receptor, Ccr9. This occurs via direct binding of Cbfβ2 to cell type–specific enhancers, as is observed in Rorγt induction during differentiation of lymphoid tissue inducer cells by activation of an intronic enhancer. As in mice, an alternative splicing event in zebrafish generates a Cbfβ2-specific mRNA, important for *ccr9* expression. Thus, despite phylogenetically and ontogenetically variable sites of origin of T cell progenitors, their robust thymus-homing capacity is ensured by an evolutionarily conserved mechanism emerging from functional diversification of Runx transcription factor complexes by acquisition of a novel splice variant.

Journal of Experimental Medicine

INTRODUCTION

T cell development is essential for cellular immunity and is initiated in the thymus. When multipotent hematopoietic precursors come into contact with the thymic stromal microenvironment, they gradually commit to the T-lymphoid lineage (Yang et al., 2010; Yui and Rothenberg, 2014). In all vertebrates, early thymic progenitors (ETPs) are generated outside of the thymus; hence, they must acquire the capacity to home to the thymus to ensure productive T cell development (Boehm and Bleul, 2006; Liu et al., 2006; Zhang and Bhandoola, 2014). In the mouse, for instance, ETPs originate in the fetal liver, and, after birth, in the bone marrow. In teleost fish, in contrast, thymus homing progenitors first develop in the caudal hematopoietic tissue and later in the kidney (Boehm et al., 2012). To cope with the complex functional requirements arising from the diverse anatomical origin of T cell progenitors, vertebrates have evolved a general mechanism that underlies thymus homing. It is based on the formation of chemotactic gradients emanating from the thymus microenvironment that are sensed by thymic progenitors via specific chemokine receptors.

Previous studies in mice have revealed a crucial role of the chemokine receptor Ccr9 during thymus homing, with contributions of Ccr7 and Cxcr4 chemokine receptors (Uehara et al., 2002; Liu et al., 2006; Jenkinson et al., 2007; Krueger et al., 2010; Zlotoff et al., 2010; Calderón and Boehm, 2011; Zhang and Bhandoola, 2014). These chemokine receptors confer responsiveness to the Ccl25, Ccl19/21, and Cxcl12 chemokines, respectively, that are secreted by thymic epithelial cells. Chemotactic cues are important not only in mice, but also guide the homing process in zebrafish, and other teleosts, with ccr9 again being the most important determinant (Bajoghli et al., 2009; Hess and Boehm, 2012). Expression of a conserved set of chemokine receptors on T cell progenitors thus appears to be an ancient evolutionary innovation (Bajoghli et al., 2009) that affords vertebrates with phylogenetic and ontogenetic flexibility with respect to the anatomical origin of T cell progenitors. Despite the crucial role of thymus homing, little is known about the transcriptional program that regulates the expression of chemokine receptors that guide the homing process.

Runx proteins are evolutionally conserved transcriptional regulators that play numerous roles during develop-

*M. Tenno and S. Kojo contributed equally to this paper.

Correspondence to Ichiro Taniuchi: ichiro.taniuchi@riken.jp

H. Kawamoto's present address is Dept. of Immunology, Institute for Frontier Medical Sciences, Kyoto University, Kyoto, Japan.

The Rockefeller University Press
J. Exp. Med. 2018 Vol. 215 No. 2 595–610
https://doi.org/10.1084/jem.20171221

ment of multiple hematopoietic cells (de Bruijn and Speck, 2004; Braun and Woollard, 2009). In mammals, three Runx family genes encoding Runx1, Runx2, and Runx3 proteins have been identified, and there are two *Drosophila* genes encoding Runx orthologues, Runt and Lozenge. To exert their functions as transcriptional regulators, all Runx proteins need to associate with an evolutionarily conserved β-subunit protein, designated Cbfβ protein in mammals (Wang et al., 1996; Adya et al., 2000), which itself does not have DNA-binding activity. Although there are two single-exon genes encoding Cbfβ orthologues in *Drosophila* (Golling et al., 1996), only one *Cbfb* gene is present in mammalian genomes. Nonetheless, distinct splice donor signals within exon 5 of the mammalian *Cbfb* genes produce two variants, Cbfβ1 and Cbfβ2, which possess distinct C-terminal amino acid sequences (Ogawa et al., 1993; Wang et al., 1993). Both Cbfβ1 and Cbfβ2 variants interact equally with Runx proteins, through a domain in the shared N-terminal part of Cbfβ (Ogawa et al., 1993; Zaiman et al., 1995). On the other hand, Crl-1 was identified as a specific Cbfβ2 partner in the brain (Sakuma et al., 2001), suggesting that Cbfβ2 may have a unique regulatory function. However, the question of whether Cbfβ1 and Cbfβ2 have distinct functions has not yet been examined in vivo using the mouse model.

Here, we report that Cbfβ2 is essential for extrathymic differentiation of thymus-homing progenitors. In addition, we identify an evolutionarily conserved alternative splicing event generating Cbfβ2 as the basis for *Ccr9* activation in vertebrate hematopoietic progenitors. Collectively, our results illuminate a mechanism by which alternative splicing of pre-mRNA increased the functional diversity of Runx complexes and established new types of cellular interactions between hematopoietic and stromal cells in lymphoid organs.

RESULTS

A small thymus and impaired γδT cell development in *Cbfb*$^{2m/2m}$ mice

Two mutually exclusive splicing events connecting sequences in exons 5 and 6 in the *Cbfb* gene result in different reading frames to generate two proteins, Cbfβ1 and Cbfβ2, that share the same N-terminal region but differ in their C-terminal amino acid sequences (Fig. 1 A). To address the function of the two Cbfβ variants in mice, we generated *Cbfb*$^{1m/1m}$ and *Cbfb*$^{2m/2m}$ strains that lacked *Cbfb2* and *Cbfb1* transcript by targeted mutation of the respective splice donor signals (Fig. S1, A–C). Expression of Cbfβ1, Cbfβ2, and total Cbfβ proteins assessed by immunoblot (Fig. 1 B) and flow cytometry (Fig. S1 D) confirmed loss of Cbfβ2 and Cbfβ1 expression in *Cbfb*$^{1m/1m}$ and *Cbfb*$^{2m/2m}$ mice, respectively. Quantitative measurements by immunoblot showed that the total amounts of Cbfβ protein were lower in *Cbfb*$^{2m/2m}$ thymocytes than in *Cbfb*$^{1m/1m}$ thymocytes and ∼45% of those in *Cbfb*$^{+/+}$ thymocytes (Fig. 1 B).

In contrast to the embryonic lethality observed with a total loss of Cbfβ protein (Wang et al., 1996), *Cbfb*$^{1m/1m}$ and *Cbfb*$^{2m/2m}$ mutant mice were born alive, indicating a certain degree of functional redundancy of these two isoforms. However, the analysis of these two mouse strains also revealed tissue-specific nonredundant functions. In addition to impaired osteoblast differentiation caused by the lack of Cbfβ2 (Jiang et al., 2016), we noticed the presence of small thymi in *Cbfb*$^{2m/2m}$ but not *Cbfb*$^{1m/1m}$ mice (Fig. 1 C). Phenotypic characterization of thymocytes revealed that their CD4/CD8 expression profiles were comparable to control mice (Fig. 1 D), except that the CD25^{+}CD44^{+} subset in CD4^{-}CD8^{-} double-negative (DN) population was increased in *Cbfb*$^{2m/2m}$ mice (Fig. 1 D). However, based on the observation of intracellular TCRβ expression in *Cbfb*$^{2m/2m}$ CD25^{+}CD44^{+} DN2 cells as well as the continuous expression of CD44 on *Cbfb*$^{2m/2m}$ CD4^{+}CD8^{+} double-positive (DP) thymocytes (Fig. 1 D), inefficient repression of CD44 could account, at least in part, for the increase in the CD25^{+}CD44^{+} DN2 subset, although developmental inhibition at the DN2-to-DN3 transition was not formally excluded. Expression of c-Kit (CD117) was also not efficiently repressed in *Cbfb*$^{2m/2m}$ CD25^{+} DN cells (Fig. S1 E). Although the percentage of ETPs, which was defined as lineage-negative (Lin^{-}) CD44^{+} c-Kit^{hi} cells in this case, in CD4^{-}CD8^{-}CD25^{-} thymocytes subset was higher, the absolute number of ETPs was significantly reduced in the adult *Cbfb*$^{2m/2m}$ thymus (Fig. S1 F).

The γδ T cell compartment was more affected than the αβ T lineage in *Cbfb*$^{2m/2m}$ mice; for instance, the number of γδ T cells in the thymus was reduced by a factor of 40 (Fig. 2 A). Compared with αβ T cells, the reduction of γδ T cells was even more pronounced in peripheral tissues. In the gut intra-epithelial lymphocyte (IEL) compartment, the percentage of γδ T cells was also severely reduced in *Cbfb*$^{2m/2m}$ mice (Fig. 2 B), whereas that of αβT cells was unaffected. Furthermore, dendritic epidermal T cells (DETCs), a skin-specific unique γδ T cell subset, were completely absent in the epidermis of *Cbfb*$^{2m/2m}$ mice (Fig. 2 C), as was observed in *Runx3*-deficient mice (Woolf et al., 2007). These observations demonstrated that Cbfβ2 variant has unique and nonredundant function in generating the γδ T cell pool in mice.

Cbfβ2 deficiency in the hematopoietic compartment is responsible for the small thymus

To address whether a defect in hematopoietic cells or in the thymic microenvironment was responsible for the small thymus and impaired γδ T cell development in *Cbfb*$^{2m/2m}$ mice, we eliminated hematopoietic cells from embryonic thymi and transplanted the alymphoid lobes under the renal capsule of adult host mice. 4 wk later, the size and cell numbers in *Cbfb*$^{+/+}$ and *Cbfb*$^{2m/2m}$ donor thymic lobes grafted into *Cbfb*$^{+/+}$ hosts were similar (Fig. 3 A). In contrast, both *Cbfb*$^{+/+}$ and *Cbfb*$^{2m/2m}$ thymic lobes developing in *Cbfb*$^{2m/2m}$ hosts were smaller and contained fewer cells than the transplants in *Cbfb*$^{+/+}$ hosts (Fig. 3 A). Thymocyte compartments in the grafted lobes assessed by CD4/CD8 expression were similar in all grafts (Fig. 3 B). However, percentages of γδ T

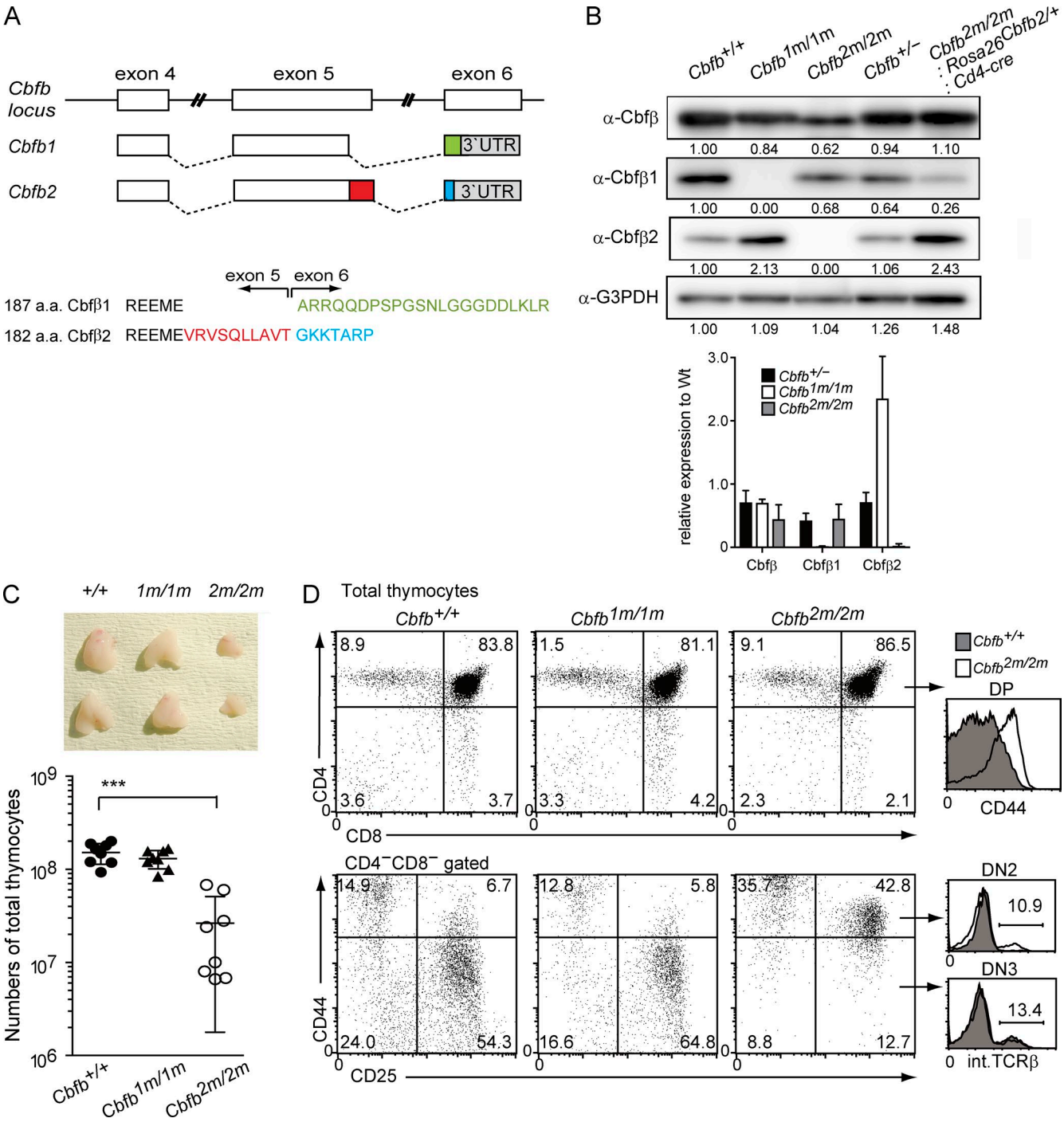

Figure 1. **Cbfβ2-specific knockout affects thymocyte numbers in mice. (A)** Structure of the mouse *Cbfb* locus that produces two splice variants by using distinct splice donor signals. The encoded Cbfβ1 and Cbfβ2 each has a distinct C-terminal amino acid sequence, which are shown in green, red, and blue. **(B)** Top: Western blots of the expression of total Cbfβ, Cbfβ1, Cbfβ2, and G3PDH proteins in total thymocytes of $Cbfb^{+/+}$, $Cbfb^{+/-}$, $Cbfb^{1m/1m}$, $Cbfb^{2m/2m}$, and $Cbfb^{2m/2m}$*: Rosa*$^{Cbfb2/+}$*:Cd4-cre* mice. Expression level of each protein relative to that in $Cbfb^{+/+}$ cells is indicated. Bottom: Summary of three quantifications is shown as the relative expression level of each Cbfβ protein in thymocytes of indicated genotypes compared with that in $Cbfb^{+/+}$ cells. Means ± SD. **(C)** Representative images of the thymi (upper) and the numbers of total thymocytes (lower) of 4–8-wk-old $Cbfb^{+/+}$, $Cbfb^{1m/1m}$, and $Cbfb^{2m/2m}$ mice. Means ± SD; ***, $P < 0.001$. **(D)** Upper and lower dot plots showing representative CD4/CD8 expression by total thymocytes and CD44/CD25 expression in the $CD4^-CD8^-$ DN subset, respectively. Numbers in each quadrant indicate percentage cells in each. Upper and lower histograms at the right showing CD44 expression by $CD4^+CD8^+$ DP thymocytes and intracellular TCRβ expression in $CD44^+CD25^+$ DN2 and $CD44^-CD25^+$ DN3 cells from $Cbfb^{+/+}$ (shaded) and $Cbfb^{2m/2m}$ (open) mice.

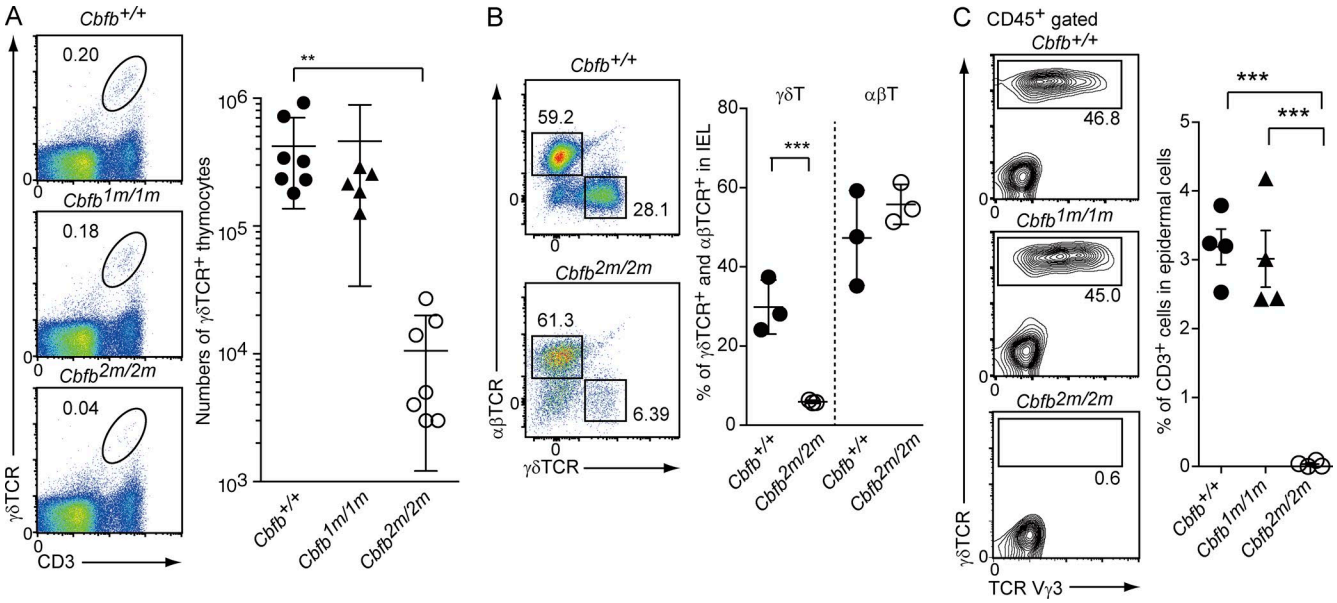

Figure 2. **Impaired γδT cell development by loss of Cbfβ2. (A)** Representative pseudocolor plots showing CD3/γδTCR expression by total thymocytes (left) and the numbers of γδT cells in the thymus (right) of *Cbfb*$^{+/+}$ (●), *Cbfb*$^{1m/1m}$ (▲), and *Cbfb*$^{2m/2m}$ (○) mice. Mean ± SD; **, P < 0.01. **(B)** Representative pseudocolor plots showing αβTCR and γδTCR expression by IELs of small intestines (left) and the percentage of γδT cells and αβT cells in IELs of *Cbfb*$^{+/+}$ (●) and *Cbfb*$^{2m/2m}$ (○) mice. Mean ± SD; ***, P < 0.001. **(C)** Representative pseudocolor plots showing TCRVγ3 and γδTCR expression by skin epidermal CD45$^+$ cells (left) and the percentage of CD3$^+$ cells in total epidermal cells of *Cbfb*$^{+/+}$ (●), *Cbfb*$^{1m/1m}$ (▲), and *Cbfb*$^{2m/2m}$ (○) mice. Mean ± SD; ***, P < 0.001. Numbers in dot plots indicate percentage cells in the indicated gate.

cells were decreased in *Cbfb*$^{2m/2m}$ recipients (Fig. 3 B). There are two pathways for the reconstitution of γδ T cells in the grafted lobes, de novo γδ T cell differentiation arising from ETPs immigrating into the grafted lobe and immigration of circulating mature γδ T cells into the graft. Although these two pathways were not formally distinguished by our approach, the more severe reduction of γδ T cells in the peripheral tissues of *Cbfb*$^{2m/2m}$ recipients suggested that the latter pathway should be responsible at least to some extent for decreased percentages of γδ T cells in *Cbfb*$^{2m/2m}$ recipients. In any case, the results of reciprocal grafting experiments indicated that the Cbfβ2-deficient thymic microenvironment can support the development of αβ T lineage from host-derived ETPs.

Consistent with these findings, competitive repopulation assays performed by injection of equal numbers of bone marrow Lin$^-$Sca-1$^+$c-Kit$^+$ (LSK) cells into sublethally irradiated Rag1-deficient recipients demonstrated a decreased ratio of *Cbfb*$^{2m/2m}$ (CD45.2) cells versus *Cbfb*$^{+/+}$ (CD45.1) cells, specifically among T-lineage cells (Fig. 3 C and Fig. S2 A). Collectively, these data indicate the presence of a hematopoietic, rather than a thymic stromal, defect in *Cbfb*$^{2m/2m}$ mice.

This conclusion is further supported by the outcome of parabiosis experiments, in which a shared blood circulation after surgical connection allows for the exchange of circulating hematopoietic cells. As a result of their high turnover, the percentages of CD45.1 and CD45.2 B lymphocytes in the spleen was found to be ∼50% in the two types of parabionts (Fig. S2 B). The same outcome was not seen in the thymus, owing to the slow turnover of cells in this organ (Donskoy and Goldschneider, 1992). In the thymi of *Cbfb*$^{+/+}$ CD45.1 and *Cbfb*$^{+/+}$ CD45.2 pairs, only ∼5% of thymocytes were exchanged over the course of the experiment. Interestingly, however, in parabiotic pairs between *Cbfb*$^{+/+}$ CD45.1 and *Cbfb*$^{2m/2m}$ CD45.2 mice, the percentages of CD45.1 cells increased in the thymus of the *Cbfb*$^{2m/2m}$ CD45.2 mice (Fig. 3 D), indicating that there were more vacant niches capable of accepting circulating thymus homing progenitors in the *Cbfb*$^{2m/2m}$ thymus. Collectively, these observations raised the possibility that the impaired thymic homing capacity in prethymic progenitors during embryogenesis may contribute to the formation of lymphopenic thymi in *Cbfb*$^{2m/2m}$ mice.

Impaired differentiation of thymic-homing progenitors in *Cbfb*$^{2m/2m}$ fetal liver

In mice, prethymic progenitors originating from fetal liver begin their migration to and colonization of the thymus anlagen at around embryonic day 11.5 (E11.5; Owen and Ritter, 1969). Consistent with the presence of much fewer Ikaros$^+$ hematopoietic cells in histological analyses (Fig. 4 A), reduction in thymocyte numbers in *Cbfb*$^{2m/2m}$ embryonic thymi was already observed by E14.5 and confirmed at E16.5 (Fig. 4 B). As a consequence, the thymic microenvironment also does not develop properly (Fig. 4 A), presumably owing to lack of lymphotoxin β and other TNF-family ligands furnished to thymic epithelial cells by developing thymocytes (Boehm et al., 2003; Akiyama et al., 2008). In the thymus of E18.5 *Cbfb*$^{2m/2m}$ embryos, Vγ3$^+$

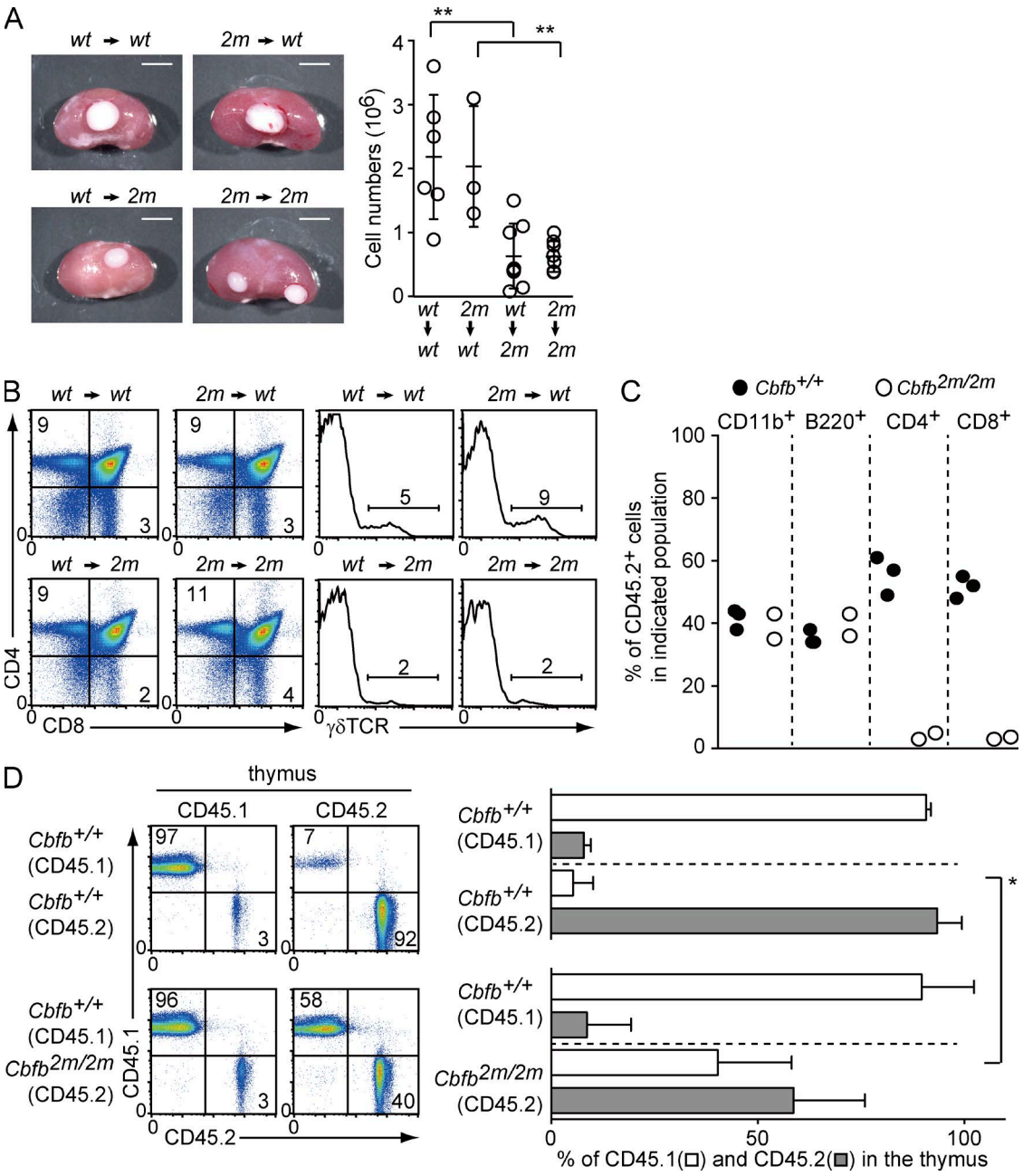

Figure 3. **Loss of Cbfβ2 in hematopoietic cells is responsible for the decrease in thymocyte numbers. (A)** Representative images of implanted *Cbfb*$^{+/+}$ (*wt*) and *Cbfb*$^{2m/2m}$ (*2m*) embryonic thymic lobes in host mice (left) and cell numbers in implanted lobes (right). Means ± SD; **, P < 0.01. Bars, 250 µm. **(B)** Pseudocolor plots showing CD4/CD8 and γδTCR expression in the implanted thymi. One representative of at least three implanted thymi. **(C)** Graph showing summary of competitive repopulation assay at least in two sublethally irradiated Rag1-deficient recipients. LSK cells from bone marrow of adult CD45.2 *Cbfb*$^{+/+}$ (●) or *Cbfb*$^{2m/2m}$ (○) mice were mixed with equal numbers (1.25×10^4) of CD45.1 *Cbfb*$^{+/+}$ LSK cells and injected into sublethally irradiated host mice. Expression of CD45.1 and CD45.2 markers on indicated cell subsets in peripheral blood was examined 40 d after injection. **(D)** Representative pseudocolor plots showing CD45.1/CD45.2 expression by thymus of each mouse in the indicated pair of parabiont (left). Numbers in the dot plots indicate the percentage of cells in each quadrant. Summary of the percentage of CD45.1 and CD45.2 cells in the thymus in three pairs of parabionts (right). Means + SD; *, P < 0.05.

cells, the known precursors for DETCs arising during embryogenesis (Payer et al., 1991), as well as other γδTCR subsets, were almost absent (Fig. 4 C), consistent with the lack of DETCs in the epidermis of adult *Cbfb*$^{2m/2m}$ mice (Fig. 2 C). Given that differentiation of Vγ3$^+$ cells in the fetal thymus was not significantly impaired under conditions of *Runx3* defi-

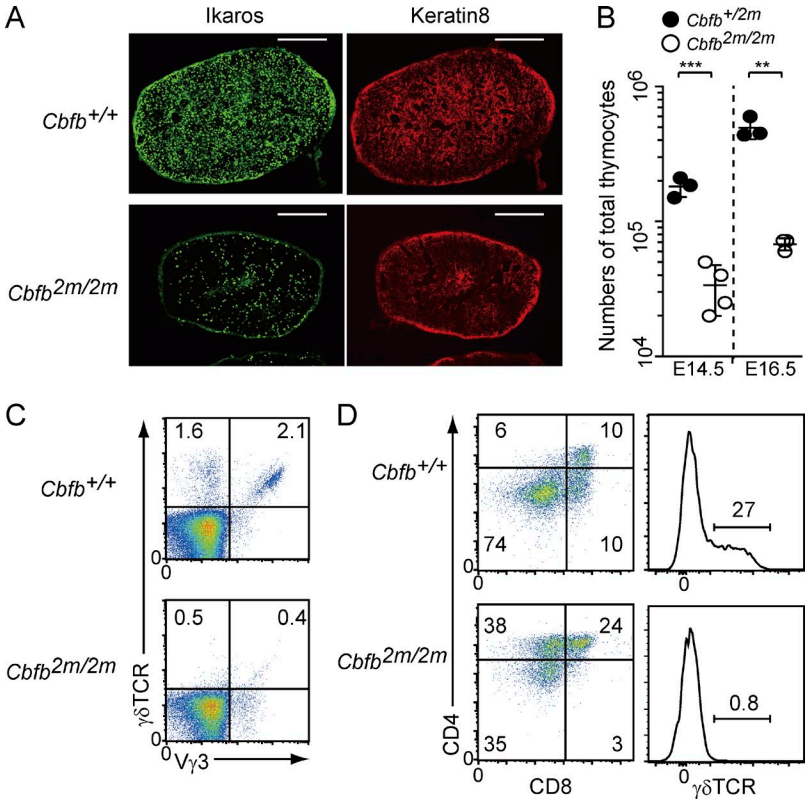

Figure 4. **Impaired thymic homing capacity in *Cbfb*$^{2m/2m}$ embryos. (A)** Representative images of fluorescent immunohistochemical staining for Ikaros$^+$ hematopoietic cells and Keratin 8$^+$ thymic epithelial cells in E14.5 thymi of *Cbfb*$^{+/+}$ and *Cbfb*$^{2m/2m}$ embryos. One representative of at least three thymi of each genotype. On representative of three samples. Bars, 100 µm. **(B)** Total numbers of E14.5 and E16.5 thymocytes from *Cbfb*$^{+/2m}$ (●) and *Cbfb*$^{2m/2m}$ (○) mice. Mean ± SD; **, $P < 0.05$; ***, $P < 0.01$. **(C)** Pseudocolor plots showing γδTCR and Vγ3$^+$ expression in E18.5 fetal thymi. Representatives of at least three independent embryos are shown. **(D)** In vitro differentiation into T-lineage cells on Tst4-expressing Delta-1 stromal cells from LSK cells prepared from E13.5 fetal livers of *Cbfb*$^{+/+}$ and *Cbfb*$^{2m/2m}$ embryos. One representative result of three cultures is shown. Numbers in the pseudocolor plots and histograms indicate the percentage of cells in each quadrant or region.

ciency (Woolf et al., 2007), Cbfβ2 must be involved in a process generating Vγ3$^+$ cells in a *Runx3*-independent manner.

We next examined hematopoiesis in the fetal liver. The LSK population in *Cbfb*$^{2m/2m}$ fetal livers was increased twofold (Fig. S2 C), consistent with an increase in colony-forming activity among *Cbfb*$^{2m/2m}$ fetal liver cells (Fig. S2 D). Increase of LSK population was also observed in adult bone marrow of *Cbfb*$^{2m/2m}$ mice (Fig. S2 E). We next examined the developmental potency of fetal liver cells in vitro. Consistent with the comparable differentiation of B220$^+$CD19$^+$ B lymphocytes in fetal liver of E12.5 *Cbfb*$^{+/+}$ and *Cbfb*$^{2m/2m}$ embryos (Fig. S2 F), B220$^+$ cells differentiated from *Cbfb*$^{2m/2m}$ Lin$^-$c-Kit$^+$ cells in vitro on Tst4 stroma cells to a similar extent as control cells (Fig. S2 G). Under T-lineage differentiation conditions on Tst4 cells expressing the Notch ligand Delta-1, both *Cbfb*$^{2m/2m}$ and *Cbfb*$^{+/+}$ progenitors differentiated into CD4$^+$CD8$^+$ DP cells (Fig. 4 D), although there was an increase in CD4$^+$CD8$^-$ cells arising from *Cbfb*$^{2m/2m}$ progenitors, presumably because of impaired *Cd4* repression, which is a well-known function of Runx complexes during T cell development (Taniuchi et al., 2002). In contrast, γδ T cells did not develop from *Cbfb*$^{2m/2m}$ progenitors (Fig. 4 D). Thus, in contrast to the cell-intrinsic block of γδ T development observed under these in vitro conditions, the *Cbfb*$^{2m/2m}$ prethymic progenitors retained the ability to become αβ T cells. Together with low number of hematopoietic cells in thymus anlagen, this result prompted us to next examine the thymic-homing capacity of *Cbfb*$^{2m/2m}$ prethymic progenitors in more detail.

Impaired differentiation of extrathymic T cell progenitors in *Cbfb*$^{2m/2m}$ mutant mice

Paired immunoglobulin–like receptor (PIR) expression marks fetal liver progenitors that possess high T-lymphoid lineage differentiation potency as well as thymus-homing capacity (Masuda et al., 2005). In the Lin$^-$c-Kit$^+$ fetal liver population of E12.5 *Cbfb*$^{2m/2m}$ embryos, the percentage and absolute numbers of IL7R$^+$PIR$^+$ cells were lower than in *Cbfb*$^{+/+}$ and *Cbfb*$^{1m/1m}$ embryos (Fig. 5 A and Fig. S3 A). Of note, in wild-type mice, the amount of Cbfβ2 is higher in IL7R$^+$PIR$^+$ cells than in IL7R$^-$PIR$^-$ cells (Fig. S3 B). To further address the roles of Runx/Cbfβ2 complexes in the differentiation of IL7R$^+$PIR$^+$ cells, we compared gene expression profiles by digital RNA-sequencing (RNA-seq; Shiroguchi et al., 2012). Interestingly, we found that *Ccr9* induction was significantly impaired in *Cbfb*$^{2m/2m}$ cells (Fig. 5 B). Consistent with high T-lineage potency in IL7R$^+$PIR$^+$ cells (Masuda et al., 2005), the amount of *Notch1* transcript was higher in IL7R$^+$PIR$^+$ cells than IL7R$^+$PIR$^-$ cells. However, in contrast to *Ccr9*, *Notch1* induction was unaffected by lack of Cbfβ2. Decreased levels of *Ccr9* mRNA were confirmed at the protein level by a significant reduction of the CCR7$^-$CCR9$^+$ subset in the E12.5 *Cbfb*$^{2m/2m}$ IL7R$^+$PIR$^+$ fetal liver population (Fig. 5 A).

Differential bindings of Runx/Cbfβ2 complexes in progenitors

To gain insight into how Runx/Cbfβ complexes are involved in regulation of *Ccr9* expression, we next analyzed Cbfβ bind-

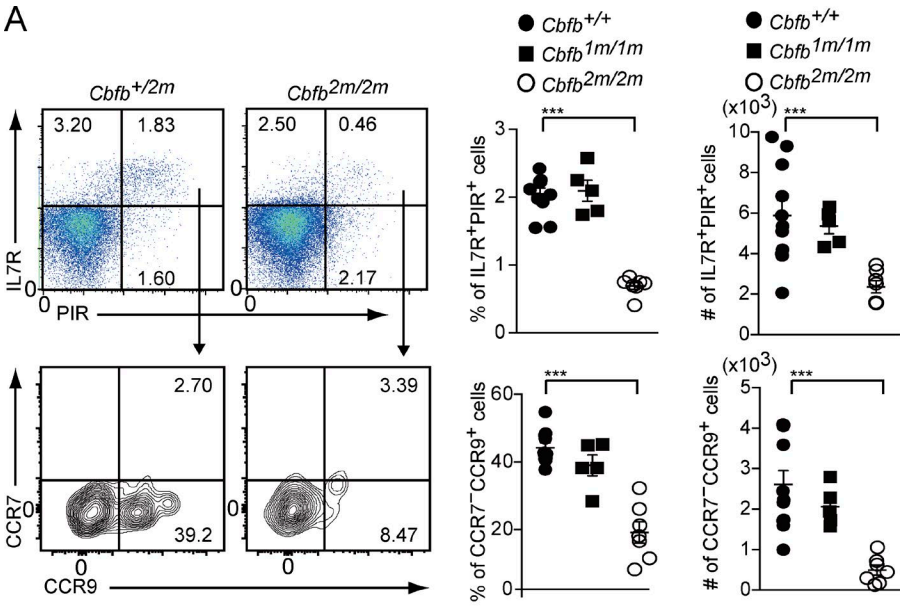

Figure 5. **Impaired differentiation of Lin⁻c-Kit⁺IL7R⁺PIR⁺ fetal liver cells expressing CCR9 in *Cbfb*$^{2m/2m}$ embryos. (A)** Representative pseudocolor plots showing PIR and IL7R expression (top) by E12.5 Lin⁻c-Kit⁺ fetal liver cells and contour plots showing CCR9 and CCR7 expression (bottom) by IL-7R⁺PIR⁺ fetal liver cells of *Cbfb*$^{+/2m}$ and *Cbfb*$^{2m/2m}$ embryos. Graphs at the right show summary of the percentage (left) of IL7R⁺PIR⁺ cells in Lin⁻c-Kit⁺ cells and CCR7⁻CCR9⁺ cells in IL7R⁺PIR⁺ cells and the absolute numbers (right) of those cells of *Cbfb*$^{+/+}$ (●), *Cbfb*$^{1m/1m}$ (■), and *Cbfb*$^{2m/2m}$ (○) mice. Means ± SD; ***, P < 0.001. **(B)** Summary of three measurements of digital RNA-sequencing showing a list of selective genes, such as *Ccr9* and *Notchl*, whose expression is up-regulated in Lin⁻c-Kit⁺IL7R⁺PIR⁺ cells.

B

	IL7R⁺PIR⁺		IL7R⁺PIR⁻		p-value +/+	p-value IL7R⁺PIR⁺
	+/+	2m/2m	+/+	2m/2m	PIR⁺ > PIR⁻	+/+ >2m/2m
Ccr9	66	22	2.2	2.8	3.9 E-18	2.1 E-11
Id2	54	20	0.78	0.87	1.6 E-16	1.5 E-8
Cbfb	50	15	35	13	8.5 E-1	1.4 E-11
Notchl	58	60	14	28	1.1 E-7	7.1 E-1

ing sites by chromatin immune precipitation followed by deep sequencing (ChIP-seq). Antibody recognizing both Cbfβ1 and Cbfβ2 variants, denoted pan-Cbfβ antibody, detected Cbfβ binding in two regions, at −13 and −10 kb upstream of the *Ccr9* transcriptional start site in both Lin⁻ fetal liver and total thymocytes (Fig. 6), to which E-box family proteins also bind (Krishnamoorthy et al., 2015). There are conserved Runx recognition sites (5′-PuACCACG/A-3′) in both regions (Fig. S3 C); the −13-kb region showed Runx-sites–dependent enhancer activity in an in vitro transfection assay (Fig. S3 D). These observations suggest that these regions act as cis-regulatory elements controlling *Ccr9* expression.

Global analyses of individual Runx/Cbfβ1 and Runx/Cbfβ2 binding sites detected by ChIP-seq using antibodies specific to each isoform, whose specificity in ChIP was confirmed by using Cbfβ1- or Cbfβ2-deficient cells (Fig. S3 E), revealed that Runx/Cbfβ2 complexes exhibit a distinct binding pattern in many genes, most specifically, in the Lin⁻ fetal liver fraction (Figs. 6 and 7, A and B). For instance, −13- and −10-kb regions in the *Ccr9* gene were predominantly bound by Runx/Cbfβ2 only in Lin⁻ fetal liver fraction but not in total thymocytes (Figs. 6 and 7 A). Interestingly, genes possessing such Runx/Cbfβ2-dominant peaks in Lin⁻ fetal liver included *Rorc* and *Tox* genes (Figs. 6 and 7 A), both of which encode transcription factors, Rorγt and Tox, respectively, that are essential for the development of lymphoid tissue inducer (LTi) cells (Sun et al., 2000; Aliahmad et al., 2010), a hematopoietic cell lineage required for the formation of secondary lymphoid tissues (Mebius, 2003). In the *Tcrd* and *Tcra* loci, only the delta enhancer (Eδ), but not the α enhancer (Eα), was occupied predominantly by Runx/Cbfβ2 in Lin⁻ fetal liver cells (Figs. 6 and 7 A). Lack of Runx/Cbfβ binding at the Eδ in total thymocytes was presumably caused by loss of genomic Eδ region as a result of VJ recombination events in the *Tcra* gene (Krangel, 2009). Although Runx/Cbfβ1-specific regions frequently contain sequences (5′-A/TTCC-3′) recognized by ETS transcription factors, which were shown to increase DNA binding affinity of Runx/Cbfβ complexes on enhancers (Kim et al., 1999; Gu et al., 2000), Runx sites were enriched in regions preferentially bound by Runx/Cbfβ2 complexes (Fig. 7 C). These observations indicate that the distinct C-terminal sequences in Cbfβ proteins influence the binding specificities of Runx/Cbfβ complexes.

Cell type–specific enhancers in the *Ccr9* and *Rorc* gene

To further examine the physiological relevance of the −13- or −10-kb regions, which are predominantly bound by Runx/Cbfβ2 complexes, for regulating *Ccr9* expression, we removed core sequences of either the −13- or the −10-kb region from the mouse genome (Fig. S3 C) by CRISPR/Cas9 genome editing (Zetsche et al., 2015). Upon deletion of either region, the percentage of IL7R⁺PIR⁺ cells

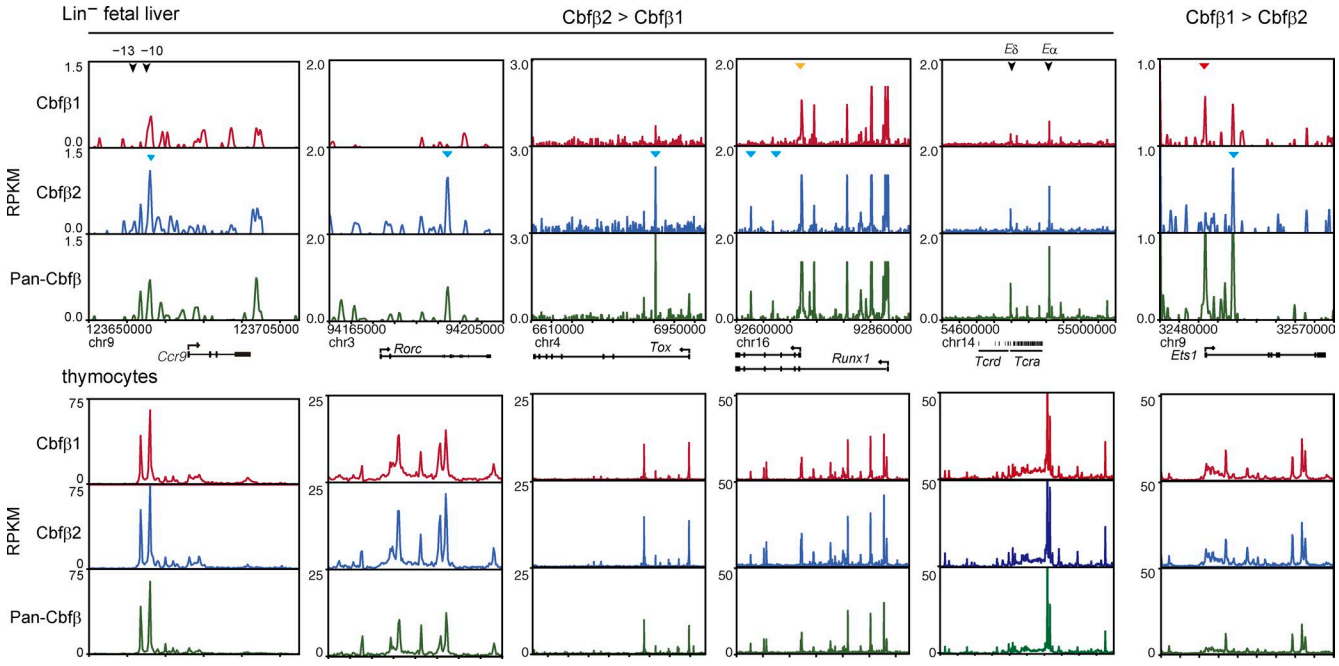

Figure 6. **Binding patterns of Runx/Cbfβ1 and Runx/Cbfβ2 complexes at selective loci.** Cbfβ variant-specific ChIP-seq tracks at the *Ccr9*, *Rorc*, *Tox Runx1*, *Tcra/d*, and *Est1* genes in E12.5 Lin⁻ fetal livers (top) and adult total thymocytes (bottom). Gene structure and transcriptional orientation are indicated at the middle. Positions of −13 kb and −10 kb regions in the *Ccr9* gene and position of the *E*δ and *E*α enhancers in *Tcrd* and *Tcra* genes, respectively, are indicated by black arrowheads. Blue, orange, and red triangles indicate regions predominantly bound by Runx/Cbfβ2, regions commonly bound by Runx/Cbfβ1 and Runx/Cbfβ2, and regions predominantly bound by Runx/Cbfβ1, respectively.

expressing CCR9 was significantly decreased (Fig. 8, A and B). Furthermore, CCR9 expression on IL7R^{+}PIR^{+} cells was abolished by the combined deletion of both regions, whereas the frequency of CCR7^{+}CCR9^{+} cells in the IL7R^{+}PIR^{-} population was unchanged even after removal of the two regions (Fig. 8, A and B).

Given a single Runx/Cbfβ2 binding to the intronic region in the *Rorc* gene in Lin^{-} fetal liver cells and requirement for Cbfβ2 in LTi cell differentiation (Tachibana et al., 2011), we next addressed how Runx/Cbfβ2 regulate *Rorc* expression. In DP thymocytes, the amount of *Rorc* assessed by RT-PCR and *Rorc*$^{+/gfp}$ reporter (Eberl et al., 2004) was decreased to approximately half in *Cbfb*$^{2m/2m}$ DP thymocytes (Fig. 8 C and Fig. S4 E). To address function of the Cbfβ2-bound intronic region, we removed it from the *Rorc*^{gfp} reporter allele. Upon its complete loss in a *Rorc*$^{gfp:\Delta E\text{-}11}$ allele (Fig. S4 A), Rorγt-gfp expression in LTi and ILC3 cells was abolished, whereas expression in DP thymocytes was retained at the half level (Fig. 8 D and Fig. S4 B). Interestingly, reduction of Rorγt-gfp from a *Rorc*$^{gfp:\Delta E\text{-}15}$ allele, in which a genomic region containing one Runx site was retained (Fig. S4 A), was milder in DP thymocytes and ILC3 (Fig. 8 D and Fig. S4 B), whereas in LTi cells it was abolished. These observations indicated that the −13- and −10-kb regions in the *Ccr9* gene and an intronic region in the *Rorc* gene act as cell type–specific and Runx/Cbfβ2-dependent enhancers to induce *Ccr9* and *Rorc* expression in PIR^{+} and LTi cells, respectively.

Although reexpression of Cbfβ2 in *Cbfb*$^{2m/2m}$ thymocytes from the *Rosa26*^{Cbfb2} locus (Tenno et al., 2017) in *Cbfb*$^{2m/2m}$:*Rosa26*$^{Cbfb2/+}$:*Cd4-Cre* mice (Fig. 1 B) restored total Cbfβ bindings to enhancers in the *Ccr9* and *Rorc* genes with reducing Cbfβ1 bindings (Fig. 7 D), it failed to completely restore thymocyte numbers and amount of *Rorc* expression (Fig. S4, C and E), whereas de-repression of CD44 in DP thymocytes was restored (Fig. S4 D). These observations suggest a possible stage-specific requirement for Cbfβ2 in activating the intronic enhancer.

Functionally conserved role of Cbfβ2 in zebrafish

Comparative analyses of gene sequences indicated that teleost fishes, instead of using an internal splice donor site in exon 5, generate the Cbfβ2 variant by using an additional exon (Fig. S5). To examine whether, despite changes in gene structures, the role of Cbfβ2 in the regulation of *ccr9* expression is evolutionarily conserved, we examined the homing capacity of hematopoietic progenitors under conditions of Cbfβ2 knockdown in zebrafish. This was achieved by use of splice site-specific antisense oligonucleotides, which suppress the formation of the *Cbfb2* transcript (Fig. 9, A and B). A previously established sensitive in vivo homing assay (Hess and Boehm, 2012) indicated drastically reduced numbers of hematopoietic cells migrating into the thymic anlage of morphants (Fig. 9 C). This effect was accompanied by decreased expression of *Ccr9a*, but not *Ccr9b* (Fig. 9 D), in line with

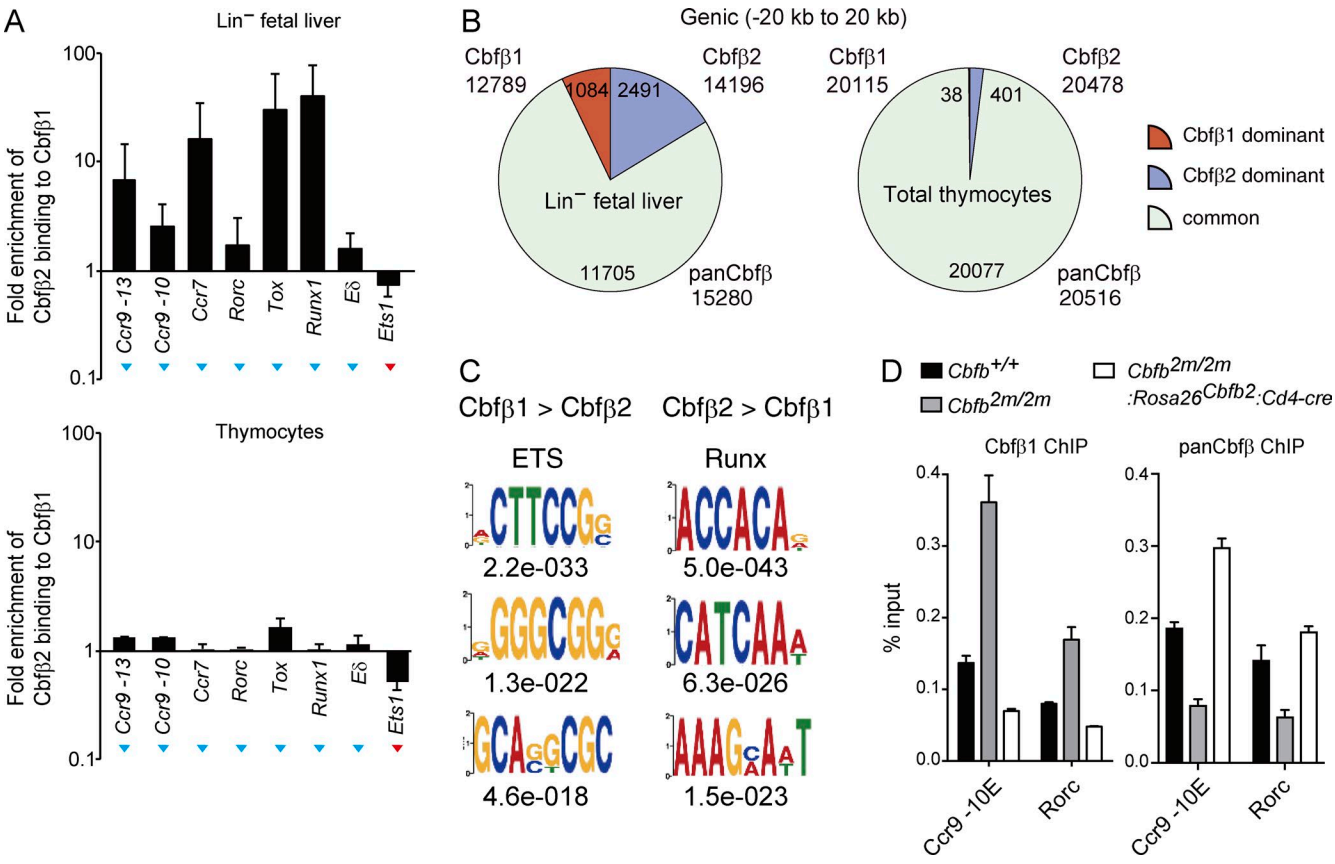

Figure 7. **Unique bindings of Runx/Cbfβ2 complexes in fetal liver progenitors. (A)** ChIP-qPCR analyses showing fold enrichment of Runx/Cbfβ2 binding signals to Runx/Cbfβ1 binding signals in Lin⁻ fetal liver cells (top) and adult total thymocytes (bottom) at selective regions where either Cbfβ1 or Cbfβ2 dominant bindings were detected by ChIP-seq as shown in red and blue triangles in Fig. 6. Cbfβ1 and Cbfβ2 binding signals were normalized to that at the *Runx1 proximal promoter* region indicated with an orange triangle in Fig. 6, where equal bindings of Cbfβ1 and Cbfβ2 were detected by ChIP-seq, and then were compared. Summary of three independent ChIP-qPCRs are shown as mean ± SD. **(B)** Pie charts showing the number of genic regions, which were defined as ±20 kb from transcription start sites (TSS), bound predominantly by Cbfβ1 or Cbfβ2 and regions commonly bound by both in E12.5 Lin⁻ fetal liver cells (left) and adult total thymocytes (right). **(C)** Motif analyses of regions preferentially bound by Cbfβ1 and Cbfβ2 in Lin⁻ fetal liver cells. The top three motifs are shown with *p*-values. ETS (5′-A/TTCC-3′) and Runx (5′-PuACCACG/A-3′) recognition sites are significantly enriched in regions bound predominantly by Cbfβ1 and Cbfβ2, respectively. **(D)** ChIP-qPCR analyses showing Runx/Cbfβ1 and total Runx/Cbfb bindings to *Ccr9* −10-kb enhancer and *Rorc* intronic enhancer in total thymocytes of *Cbfb*$^{+/+}$, *Cbfb*$^{2m/2m}$ and *Cbfb*$^{2m/2m}$*: Rosa*$^{Cbfb2/+}$*:Cd4-cre* mice. Summary of three individual ChIP is shown as mean ± SD.

the lack of homing function of the Ccl25b/Ccr9b ligand/receptor pair (Hess and Boehm, 2012). These data suggest that Cbfβ2 is a key regulator of thymic homing not only in mice but also in zebrafish via its effect on *ccr9* expression.

DISCUSSION

Our present study revealed that Cbfβ2 plays essential roles in the generation of IL7R^{+}PIR^{+} thymus-homing progenitors in the fetal mouse liver. Inefficient reconstitution of αβT cell development in grafted thymus lobes in adult *Cbfb*$^{2m/2m}$ recipients indicates that Cbfβ2 is essential for differentiation of extrathymic progenitors in the bone marrow of adult mice or at least for endowing them with thymus-homing capacity. In addition, our results unraveled the requirement for Cbfβ2 in the activation of the mouse *Ccr9* gene, which encodes the principal thymus homing receptor, through regulating cell type–specific enhancers. We also provided evidence showing an evolutionarily conserved role of Cbfβ2 in regulating *ccr9* expression in zebrafish. Collectively, these observations establish an essential role of Cbfβ2 in orchestrating a genetic program that controls development of and confers thymus-homing capacity to prethymic progenitors in vertebrates. Inefficient T cell reconstitution in the grafted thymus lobes in adult *Cbfb*$^{2m/2m}$ recipients suggests that Cbfβ2 is likely to regulate differentiation or thymus-homing capacity of adult circulating prethymic progenitors. However, because of the lack of direct evidence by using adult prethymic progenitors, our results do not formally exclude a possibility that Cbfβ2-dependent developmental program for fetal prethymic progenitor differentiation may not hold true in adults.

Cbfβ2 is also essential for generation of γδT cells in mice. Previous work had characterized Runx/Cbfβ com-

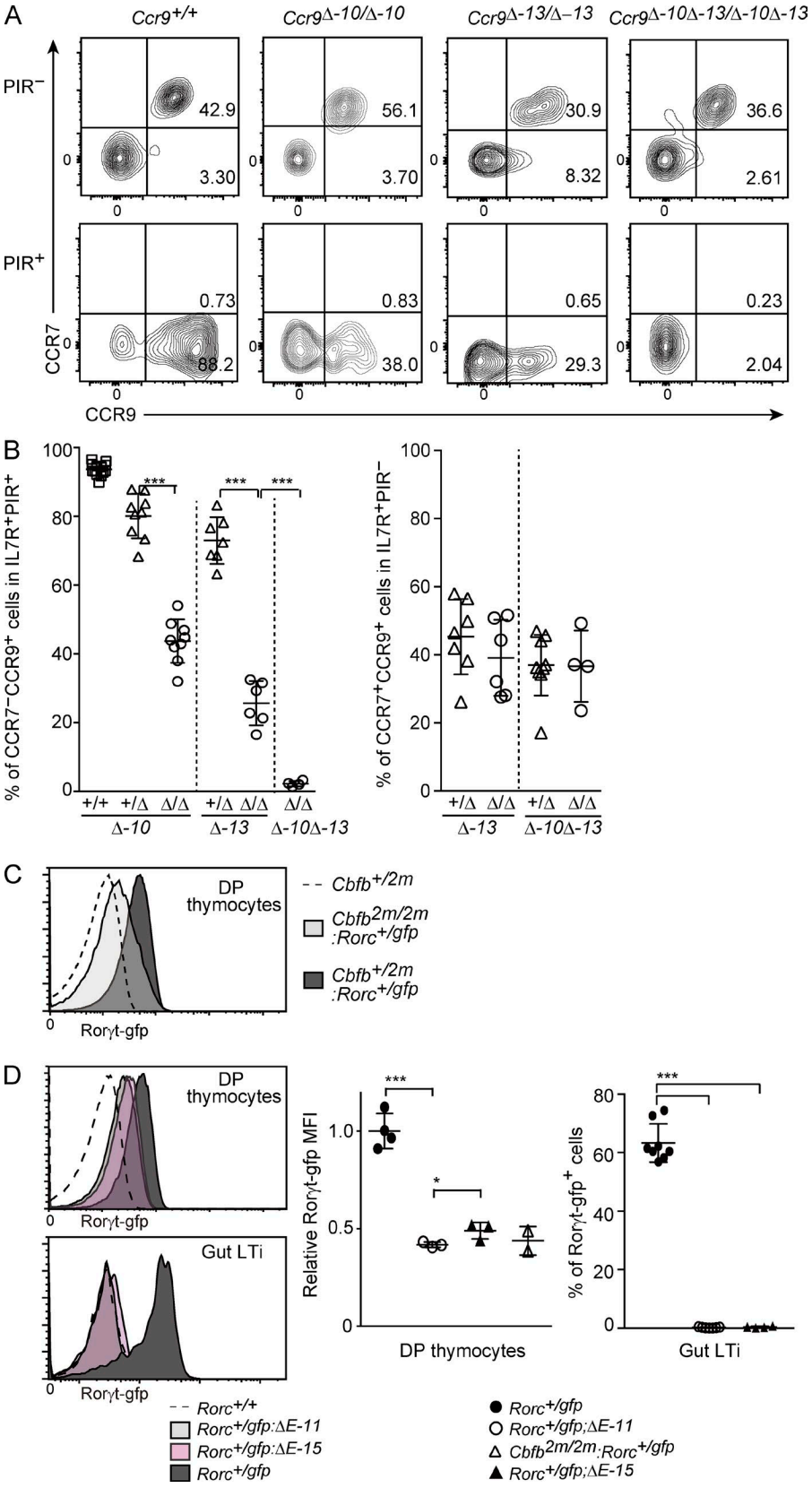

Figure 8. **Regulation of *Ccr9* and *Rorc* expression by cell type–specific enhancers. (A)** Representative contour plots showing CCR7 and CCR9 expression by IL7R$^+$PIR$^-$ and IL7R$^+$PIR$^+$ cells of E12.5 *Ccr9*$^{+/+}$, *Ccr9*$^{\Delta-10/\Delta-10}$, *Ccr9*$^{\Delta-13/\Delta-13}$, and *Ccr9*$^{\Delta-10\Delta-13/\Delta-10\Delta-13}$ Lin$^-$c-Kit$^+$ fetal liver cells. Numbers in the plots indicate the percentage of cells in each quadrant. **(B)** Summary of the percentage of the CCR7$^-$CCR9$^+$ cells among IL7R$^+$PIR$^+$ population and CCR7$^+$CCR9$^+$ cells among IL7R$^+$PIR$^-$ population of *wild-type* (+/+), heterozygous (+/Δ), and homozygous (Δ/Δ) embryos for the *Ccr9*$^{\Delta-10}$, *Ccr9*$^{\Delta-13}$, and *Ccr9*$^{\Delta-10\Delta-13}$ mutation. Means ± SD; ***, P < 0.001 (unpaired Student's *t* test). **(C)** Representative histograms showing Rorγt-gfp expression from the *Rorc*^{gfp} allele in CD4$^+$CD8$^+$ DP thymocytes of *Cbfb*$^{+/2m}$, *Cbfb*$^{+/2m}$: *Rorc*$^{+/gfp}$, and *Cbfb*$^{+/2m}$: *Rorc*$^{+/gfp}$ mice. **(D)** Representative histograms showing Rorγt-gfp expression from *Rorc*$^{+}$, *Rorc*$^{gfp:\Delta E-11}$, *Rorc*$^{gfp:\Delta E-15}$, and *Rorc*$^{+/gfp}$ alleles in CD4$^+$CD8$^+$ DP thymocytes and gut LTi cells defined as Lin$^-$IL7Ra$^+$α4β7$^+$ intestinal lamina propria cells of 18.5 days postcoitum (dpc) embryos. Graphs showing summary of relative mean fluorescence intensity (MFI) of Rorγt-gfp in DP thymocytes and percentage of Rorγt-gfp expressing cells in Lin$^-$IL7Ra$^+$α4β7$^+$ population. Means ± SD; ***, P < 0.001; *, P < 0.05 (unpaired Student's *t* test).

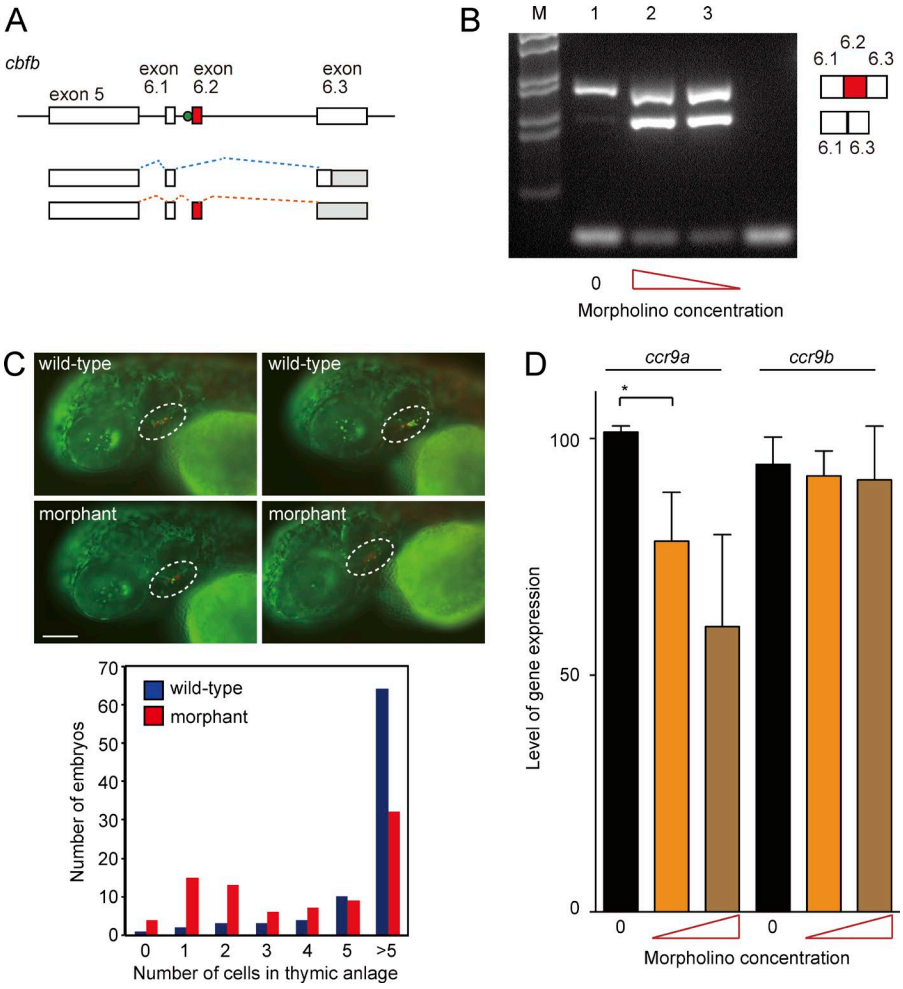

Figure 9. **Reduced expression of *ccr9a* genes in zebrafish by knockdown of the Cbfβ2 variant. (A)** Schematic of the splicing pattern of the zebrafish *cbfb* gene, with the targeted splice acceptor site indicated by a green dot. Open boxes and gray boxes represent the coding and 3′ untranslated region (3′ UTR), respectively. Exon 6.2 marked with a red box encodes Cbfβ2-specific sequences. **(B)** RT-PCR demonstrating exon skipping as a function of morpholino concentration in the injection buffer (lane 1, 0 µM; lane 2, 200 µM; lane 3, 100 µM). The structures of the PCR products were verified by sequencing. **(C)** Analysis of thymus homing in double-transgenic zebrafish (*ikaros*:*eGFP* and *foxn1*:*mCherry*) that were injected with *Cbfb2* gene-specific splice acceptor antisense morpholino oligos. At 63 hpf (hours postfertilization), the numbers of cells present in the thymic rudiments (marked with circles) was determined. Representative images of two different wild-type and morphants (top). Bar, 100 µm. Numbers of hematopoietic cells present in the thymus rudiments (bottom). The difference between wild-type and morphant was significant at $P < 0.001$. **(D)** Results of RT-qPCR for expression of *ccr9a* and *ccr9b* genes; morpholino concentrations were same as in B; $n = 3$ per condition. Mean ± SD; *, $P < 0.05$ (unpaired Student's *t* test).

plexes as primary factors that induce a conformational change of *Eδ* enhancer to augment binding of other transcription factors, such as c-Myb (Hernández-Munain and Krangel, 2002). However, the molecular basis of such structural functions of Runx/Cbfβ complexes had remained unclear. For the first time, our results clearly demonstrate that Runx/Cbfβ1 and Runx/Cbfβ2 complexes have distinct binding patterns in significant numbers of genes, mainly in fetal liver progenitor cell populations. The preferential binding of Cbfβ2 to the Eδ enhancer already in Lin^- fetal liver cells suggests that Runx/Cbfβ2 complexes function as the primary factor to initiate structural changes at the Eδ enhancer, which allows for the subsequent recruitment of other factors when ETPs are exposed to environmental cues that induce γδ T cell development. Of note, late expression of Cbfb2 is not sufficient to restore Rorγt expression in DP thymocytes. Thus, it is possible that Runx/Cbfβ2 functions as a structural factor at specific developmental stages. Compared with progenitor stages, the differential binding characteristics of Runx/Cbfβ1 and Runx/Cbfβ2 complexes at these enhancers are lost in cells at later developmental stages. It is possible that Runx/Cbfβ1 complexes can be recruited to these enhancers after conformational changes of the target loci or the tethering of multiple enhancer binding proteins that occur during or after a Cbfβ2-dependent priming of enhancer activation. Nevertheless, it is conceivable that acquisition of unique C-terminal sequences in Cbfβ2 modulates the functionality of Cbfβ proteins to become more potent to initiate enhancer activation. Given that amounts of Cbfβ2 are increased in the $IL7R^+PIR^+$ subset, it is also possible that the Cbfβ2 amount is important for increase in the efficacy of enhancer activation during differentiation of prethymic T cell progenitors. Nevertheless, it will be important in future studies to isolate molecules that associate predominantly or specifically with Runx/Cbfβ2 complexes.

Functional diversification of cell and organ systems during the course of evolution is often associated with changes in the expression characteristics and/or the protein structures of transcriptional regulators (Teichmann and Babu, 2004; Baker et al., 2012). Comparative genome analyses suggest that alternative pre-mRNA splicing events at the *Cbfb* gene giving rise to a variant C-terminal sequence of the Cbfβ protein emerged as early as bony fish, and perhaps even earlier than that. Our results thus illustrate how the emergence of

the Cbfβ2 variant supported the evolution of a robust chemotactic mechanism of thymus homing, which represents a rate-limiting step in T cell development. This evolutionary innovation thus endowed vertebrates with enormous developmental flexibility with respect to the anatomical origins of T cell progenitors, ranging from appendages of the esophagus to bone marrow (Boehm et al., 2012). We note that the functional plasticity of Runx transcription factor complexes described here also underlies a second major innovation in the adaptive immune system of vertebrates. Runx1/Cbfβ2 complexes are required for the differentiation of LTi cells (Tachibana et al., 2011). Our results demonstrated that a single intronic enhancer is crucial for *Rorc* induction in LTi and ILC3 cells, whereas *Rorc* expression in DP thymocytes was only partially reduced. In addition, Cbfβ2 is known to be essential for efficient induction of α4β7 integrin during LTi differentiation (Tachibana et al., 2011), which serves as a homing receptor for LTi cells to better interact with mesenchymal lymphoid organizer (LTo) cells at the sites where second lymphoid tissues are formed (Mebius et al., 1996; Mebius, 2003). We therefore speculate that the ancestral regulatory mechanisms that evolved to support the formation of the primary lymphoid organ, the thymus, were coopted at a later stage in evolution to support differentiation of LTi cells and endow them with a unique homing capacity underlying the generation of secondary lymphoid tissues. Collectively, our results illustrate how an increase in the functional diversity of transcription factors by alternate RNA splicing was exploited to generate diverse types of immune tissues, presumably by increasing the probability of enhancer activation associated with cell type–specific genes.

MATERIALS AND METHODS

Generation of *Cbfb*^{1m} and *Cbfb*^{2m} mutant mouse strain and other mice

1 kb of 5′ short homology genomic region was amplified by PCR to add NotI site at the 5′ end and SalI site at the 3′ end. After sequence verification in the pCRII-TOPO vector (Invitrogen), a DNA fragment encoding the *neomycin resistant gene (neo*^{r}*)* flanked by loxP sequences was prepared from the pL2Neo(2) vector and inserted into the SalI site. DNA fragments containing the desired *Cbfb*^{1m} and *Cbfb*^{2m} mutations were generated by overlap PCR and sequenced in the pCRII-TOPO vector, thereby generating the pCRTOPO-B1KO or pCRTOPO-B2KO vectors, respectively. A 7.5-kb SacI-KpnI fragment used as a 3′ long homology region was prepared by restriction enzyme digestion from the targeting vector used for generating the *Cbfb*^{flox} mutation (Naoe et al., 2007). This fragment was inserted into SacI/KpnI sites of the pCRTOPO-B1KO and pCRTOPO-B2KO vectors. Finally, the NotI-SalI fragment containing the 5′ short homology region and the *neo*^{r} cassette were ligated into the NotI/SalI sites upstream of the 3′ long homology region. The targeting vectors were linearized by NotI digestion before transfection into the E14 ES cell line. Transfection and screening of ES clones that had undergone homologous recombination was performed as previously described (Naoe et al., 2007). *Rosa26*^{Cbfb2} transgenic mice was previously described (Tenno et al., 2017). Congenic CD45.1 C57/B6 mice and Rag1-deficient host mice were from the Jackson Laboratory. *Rorc*^{gfp} reporter mice (Eberl et al., 2004) and *Cd4-Cre* mice were from D.R. Littman (New York University, New York, NY) and C.B. Wilson (University of Washington, Seattle, WA). *Rosa26*^{Cbfb2} mice were previously described (Tenno et al., 2017). All mice were maintained in the animal facility at the RIKEN IMS, and all animal experiments were performed in accordance with guidelines for animal care approved by Institutional Animal Care and Use Committee of RIKEN Yokohama Branch.

Antibodies and Western blotting

The antibody that recognizes pan-Cbfβ protein and those specific for Cbfβ1 and Cbfβ2 variants were generated by immunizing rabbits with synthetic peptides. Sequences of the peptides are shown in Table S1. Cell lysates from total thymocytes were resolved by SDS-PAGE and transferred to Immobilon-P Transfer Membranes (Millipore). Membranes were probed with an appropriate primary antibody and HRP-conjugated secondary antibody, and immune complexes were detected using ECL Prime (GE Healthcare) with Amersham Imager 600 (GE Healthcare). Quantification analysis was performed with ImageJ software (National Institutes of Health).

Flow cytometry analyses and cell sorting

To prepare epidermal cells, ears were split into dorsal and ventral halves and incubated with 0.5% trypsin and 1 mM EDTA for 1 h at 37°C after removal of cartilage. The epidermis was peeled from the dermis and dissociated into single cells by mashing through a 70-µm cell strainer (BD Bioscience). To prepare the gut IELs, small intestines were cut into 5-mm pieces after removal of fat and Payer's patches and incubated with 5 mM EDTA and 2% FCS in HBSS medium at 37°C for 20 min with shaking. Lymphocytes in supernatants were prepared by Percoll gradient (40% and 80%). Lamina propria lymphocytes were prepared as previously described (Ebihara et al., 2015). Single-cell suspensions from thymus and lymph nodes were prepared by mashing tissues through a 70-µm cell strainer (BD Bioscience). Single-cell suspensions were stained with the following antibodies purchased from BD Bioscience or eBiosciences: CD3 (145-2C11), CD4 (RM4-5), CD8 (53-6.7), CD11b (M1/70), CD25 (PC61), CD44 (IM7), CD45.1 (A20), CD45.2 (104), CD117 (2B8), CD127 (A7R34), CCR7 (4B12), CCR9 (eBioCW-1.2), KLRG1 (2F1), NK1.1 (PK136), NKp46 (29A1.4), PIR-A/B (6C1), Sca1 (E13-161.7), B220 (RA3-6B2), Gr-1 (RB6-8C5), Ter119 (Ter119), TCRβ (H57-597), TCRγδ (GL3), Vγ3 (536), and Rorgt (B2D). For intracellular staining with antibodies, cells were permeabilized before staining. For detection of Rorgt, cells were permeabilized with Bioscience Foxp3/Transcription Factor Staining Buffer Set (00-5523-00). Multicolor flow cytometry analysis was performed using

a FACSCanto II (BD Bioscience), and data were analyzed using FlowJo (Tree Star) software. Cell subsets were sorted using a FACSAria II (BD Biosciences).

Competitive repopulation assay by generation of mixed bone marrow chimera

LSK cells from bone marrow of adult CD45.2 *Cbfb*$^{+/+}$ or *Cbfb*$^{2m/2m}$ mice were mixed with equal numbers (1.25×10^4) of CD45.1 *Cbfb*$^{+/+}$ LSK cells and injected intravenously into sublethally irradiated Rag1-deficient host mice. 40 d later, the percentages of CD45.2$^+$ and CD45.1$^+$ cells in several hematopoietic subsets in peripheral blood were analyzed by flow cytometry.

Parabiosis and implantation of embryonic thymic lobes

Matching skin incisions running from elbow to knee of the corresponding lateral aspect of adult CD45.2 *Cbfb*$^{+/+}$ or *Cbfb*$^{2m/2m}$ mice and CD45.1 *Cbfb*$^{+/+}$ were surgically joined as described previously (Donskoy and Goldschneider, 1992). After 5 mo, tissues of each mouse were dissected and analyzed by flow cytometry. Thymic lobes prepared from *Cbfb*$^{+/+}$ and *Cbfb*$^{2m/2m}$ E15.5 embryos were treated with 1.35 mM deoxyguanosine (Nacalai Tesque) on polycarbonate filters (pore size 8.0 µm; Nucleopore Co.) in RPMI 1640 supplemented with 10% FCS for 6 d and then implanted under the renal capsules of *Cbfb*$^{+/+}$ and *Cbfb*$^{2m/2m}$ adult recipient mice. 4 wk later, implanted thymic lobes were harvested and analyzed by flow cytometry.

Immunohistochemistry

Embryonic thymic lobes were embedded in OCT compound (Sakura Fine Tek) in Leica Histomolds (Leica Microsystems) and snap-frozen in liquid nitrogen. Tissues were cut into 5-µm sections using a Leica CM3050S cryostat and mounted onto MAS-coated slides (Matsunami Glass). After fixation with acetone for a few seconds, sections were incubated with primary antibodies for 1 h at room temperature, washed five times with PBS/0.05% Tween20, and incubated with secondary reagents for 30 min at room temperature.

Colony-forming assay

A colony-forming assay was conducted following the manufacturer's instructions (Stem Cell Technologies). Single-cell suspensions of total fetal liver cells from E12.5 embryos were mixed with MethoCult GF M3434 containing stem cell factor, IL-3, IL-6, and erythropoietin and plated in 6-cm dishes. Colony numbers were counted after 3 to 8 d of culture in a humidified CO_2 incubator.

Digital RNA-seq analysis

In brief, dRNA-seq for 100-cell analyses were performed by using a molecular barcoding technique (Kivioja et al., 2012; Shiroguchi et al., 2012; Ogawa et al., 2017). First, for normalization, the same amount of spike-in RNAs, a known number of External RNA Controls Consortium (ERCC) RNA molecules, was added into every tube, which contained 100 cells. Then, the cells were lysed, and RNA molecules were fragmented by temperature elevation. cDNAs were generated by reverse transcription using a reverse transcription primer in which the first common primer sequence, molecular barcode, 14 T bases, and one V (A or G or C) base were tandemly arranged from the 5′ end. In the reverse transcription, a second common primer sequence was also attached to the 3′ end of each generated cDNA molecule by template switching. Subsequently, cDNAs were amplified by PCR using two primers: one containing an Illumina adapter sequence, sample index, and the first common primer sequence; and the other containing another Illumina adapter sequence, sample index, and the second common primer sequence. The quality of the amplified product (library) was measured using a Bioanalyzer (Agilent), and the concentration was determined by qPCR (7500 Real Time PCR System; Applied Biosystems). Six libraries labeled with different sample indexes were sequenced together in a single MiSeq run (150 cycles; Illumina kit). Sequencing results were analyzed using an in-house pipeline in which TopHat2 (Kim et al., 2013) was used for mapping to the mouse genome (mm10 assembly). This strategy provides the mean number of mRNA molecules per cell for each gene and each indexed sample by counting the number of unique molecular barcodes instead of the number of sequenced cDNA molecules. Differential gene expression analysis was performed using DESeq2.

ChIP-seq

For ChIP-seq with anti-Cbfβ1, anti-Cbfβ2, or anti–pan Cbfβ antibody, 10^7 Lin$^-$ fetal liver cells from E12.5 C57BL/6N embryos and 10^7 thymocytes from 4-wk-old C57BL/6N mice were washed once with PBS containing 1% FCS and cross-linked by incubation in a 1% formaldehyde solution for 10 min with gentle rotation at room temperature. The reaction was stopped by addition of a 0.15-M (final concentration) glycine solution and 10 min gentle rotation. Cells were washed with ice-cold PBS containing 1% FCS for 10 min with gentle rotation at 4°C and lysed by incubation in Lysis Buffer 1 (50 mM Hepes, pH 7.5, 140 mM NaCl, 1 mM EDTA, 10% glycerol, 0.5% NP-40, and 0.25% Triton X-100) supplemented with cOmplete protease inhibitor cocktail tablets (Roche) for 10 min at 4°C. Nuclei were pelleted and washed by suspension into Lysis Buffer 2 (10 mM Tris-HCl, pH 8.0, 200 mM NaCl, 1 mM EDTA, and 0.5 mM EGTA) supplemented with cOmplete protease inhibitor (Roche). Nuclei were then resuspended in 300 µl Lysis Buffer 3 (10 mM Tris-HCl, pH 8.0, 100 mM NaCl, 1 mM EDTA, 0.5 mM EGTA, 0.1% sodium deoxycholate, and 0.5% *N*-laurylsarcosine sodium salt) and sonicated 10 times using a model XL2000 ultrasonic cell disruptor (Microson) at output level 6 for 15 s. After the addition of Triton X-100, sonicated chromatin was incubated overnight at 4°C with gentle rotation in the presence of anti-Cbfβ1, anti-Cbfβ2, or anti–pan Cbfβ antibody that was preconjugated with

Dynabeads M-280 Sheep anti-Rabbit IgG (Thermo Fisher Scientific). After washing beads with ChIP-RIPA (50 mM Hepes, pH 7.6, 500 mM LiCl, 1 mM EDTA, 1% NP-40, and 0.7% sodium deoxycholate) and TE buffer supplemented with 50 mM NaCl, immunoprecipitates were eluted from beads into 100 µl of Elution Buffer (50 mM Tris-HCl, pH 8.0, 10 mM EDTA, and 1% SDS) by incubation for 15 min at 65°C. Eluted immunoprecipitates were incubated at 65°C overnight for reverse cross-linking. Input DNA and ChIP DNA were treated with RNase A (Thermo Fisher Scientific) at 37°C for 1 h, followed by incubation with proteinase K (Thermo Fisher Scientific) at 55°C in the presence of 6 mM $CaCl_2$ for 1 h. DNA was extracted by phenol/chloroform, and purified DNA was subjected to resonication with a Covaris S220 to produce DNA fragments with a mean size of 200 bp, used for library construction with NEBNext ChIP-seq Library Prep Master Mix set for Illumina kit (NEB). Sequencing was performed by the RIKEN IMS sequence facility with Illumina HiSeq 1500. Sequence reads were aligned on mouse genome mm9 using bowtie2 (v.2.1.0, http://bowtie-bio.sourceforge.net/index.shtml) with default parameters. Regions preferentially bound by Cbfβ1 or Cbfβ2 (q-value < 0.05) were extracted using MACS2 (v.2.0.10, https://github.com/taoliu/MACS), and DNA sequence motifs enriched among regions preferentially bound by Cbfβ1 and Cbfβ2 were extracted by the "dreme" command included in MEME Suite (v.4.9.0, http://meme-suite.org/) using 250-bp sequences ranging from the center of binding peaks.

CRISPR/Cas9-mediated genome editing

To delete the −13- or −10-kb genomic region from the mouse *Ccr9* locus and the intronic region from the $Rorc^{gfp}$ allele by CRISPR/Cas9, two guide RNA (gRNA) sequences flanking the putative enhancer regions were selected through single guide RNA (sgRNA) Designer software at the Broad Institute (Cambridge, MA). Sequences and positions of gRNA are shown in Figs. S3 and S4. Custom gRNA, in which CRISPR RNAs (crRNAs) were fused to a normally trans-encoded tracrRNA, were transcribed from a T7 promoter in the pUC18 vector by in vitro transcription with MEGAshortscript T7 kit (Life Technologies), and both the *Cas9* mRNA and the gRNAs were purified using the MEGAclear kit (Life Technologies). The gRNAs and mRNA encoding Cas9 were coinjected into the cytoplasm of C57/B6N fertilized eggs by the Animal Facility Group at RIKEN IMS. To generate a *Ccr9* allele harboring double deletions, a −13- and −10-kb region ($Ccr9^{\Delta-10\Delta-13}$), gRNA pair used for generation of $Ccr9^{\Delta-10}$ mutation was injected into eggs obtained by in vitro fertilization between $Ccr9^{\Delta-30/\Delta-30}$ sperm and wild-type oocytes. Similarly, eggs obtained by in vitro fertilization between $Rorc^{gfp/gfp}$ sperm and wild-type oocytes were used to generate a $Rorc^{gfp}$ allele harboring deletion at the intronic region.

Morpholino oligo-mediated knockdown of *Cbfb2* in zebrafish

To selectively knock down the zebrafish *cbfb2* variant, which is composed of exon 6.1 and 6.2, we chose complementary sequences to the splice acceptor to exon 6.2 as follows: 5′-GGTCCTAAAAAACACAATTTGGTTT-3′ synthesized by Gene Tools (Philomath, OR). The morpholinos were dissolved in 1× Danieau buffer at the indicated concentrations and injected into zebrafish embryos at the one-cell stage. For injections, the morpholino was used at 100, 133, or 200 mM in injection buffer as described (Hess and Boehm, 2012). Two transgenic zebrafish lines (Hess and Boehm, 2012) were used for live imaging: the *ikaros*:*eGFP* reporter for marking lymphoid progenitor cells and the *foxn1*:*mCherry* reporter for marking the thymic epithelium. Live imaging was performed as previously described (Hess and Boehm, 2012). In brief, for long-term imaging, embryos and larvae were anesthetized with tricaine methanesulfonate, immobilized in 0.8–1% low-melting agarose, covered with embryo medium (5 mM NaCl, 0.17 mM KCl, 0.33 mM $CaCl_2$, and 0.33 mM $MgSO_4$) and kept in a heating chamber at 28°C. For short-term imaging, embryos and larvae were anesthetized and immobilized in 3% methylcellulose. Fluorescence microscopy was performed with a Zeiss Imager.Z1. 3D image analysis and cell tracking were performed with Bitplane Imaris x64 6.4.0 software. The presence of ≥5 cells per rudiment was considered to be indicative of normal colonization; hence, for statistical purposes, the fraction of embryos with 0–4 intrathymic cells was compared with those containing ≥5 cells. RT-qPCR for expression of *ccr9* paralogs was performed using primer sets purchased from Bio-Rad (assay numbers, qDreCEDOOO9932 [*ccr9a*]; qDreCED0021482 [*ccr*9b]) using an *actb1* primer set (Lam et al., 2004) as reference. Primers used for exon skipping are listed in Table S1.

Comparative genomics analyses

Information and sequences of *Cbfb* gene and its transcripts were obtained from GenBank and published manuscripts (Ng et al., 2007; Nah et al., 2014a,b). Genome sequences of elephant shark (*Callorhinchus milii*) and Japanese lamprey (*Lethenteron japonicum*) were downloaded from elephant shark genome assembly (http://esharkgenome.imcb.a-star.edu.sg/) and Japanese lamprey genome assembly (http://jlampreygenome.imcb.a-star.edu.sg/), respectively. Alignment of C-terminal sequences of Cbfβ variants of each species was performed by Clustal Omega (http://www.clustal.org/omega/) with default parameters for amino acid sequences and was curated by hand.

Data analyses and accession codes

Statistical analysis was performed by Student's unpaired t test with Prism 6 (GraphPad Software) unless otherwise stated. All sequencing datasets are deposited in the

Genome Expression Omnibus database under accession nos. GSE86850 and GSE90794.

Online supplemental materials

Fig. S1 shows the generation of *Cbfb*^{1m} and *Cbfb*^{2m} mice. Fig. S2 shows the defect in hematopoietic cells for small thymus. Fig. S3 shows information about two enhancers in the *Ccr9* gene. Fig. S4 shows information about the intronic enhancer in the *Rorc* gene. Fig. S5 shows structures of the *Cbfb* gene and its transcripts in several species. Table S1 shows sequence information for the peptide and primers used for quantitative real-time PCR, ChIP-qPCR, and exon skipping in zebrafish.

ACKNOWLEDGMENTS

We thank N. Yoza for cell sorting, K. Fukuhara for help in performing digital RNA-sequencing, and C. Miyamoto for mouse genotyping and cell preparation.

This work was supported by Grants-in-Aid for Scientific Research (S: 21229008) and (B: 19390118) from Japan Society for the Promotion of Science, Grants-in-Aid for Scientific Research on Innovative Areas (22118004) from the Ministry of Education, Culture, Sports, Science and Technology in Japan and Takeda Science Foundation (I. Taniuchi), RIKEN IMS YCI program and PRESTO from Japan Science and Technology Agency (K. Shiroguchi), and the Max Planck Society (T. Boehm).

The authors declare no competing financial interests.

Author contributions: M. Tenno performed phenotypic characterization of mutant mice. S. Kojo performed ChIP-seq. D.-F. Lawir and I. Hess performed zebrafish experiments. K. Shiroguchi performed digital RNA-seq. T. Ebihara analyzed Roryt expression in ILC3, T.A. Endo analyzed bioinformatics data, S. Muroi generated mutant mouse strains, and R. Satoh and H. Kawamoto performed histological analyses. T. Boehm and I. Taniuchi designed experiments and wrote the manuscript.

Submitted: 11 July 2017

Revised: 28 October 2017

Accepted: 13 December 2017

REFERENCES

Adya, N., L.H. Castilla, and P.P. Liu. 2000. Function of CBFbeta/Bro proteins. *Semin. Cell Dev. Biol.* 11:361–368. https://doi.org/10.1006/scdb.2000.0189

Akiyama, T., Y. Shimo, H. Yanai, J. Qin, D. Ohshima, Y. Maruyama, Y. Asaumi, J. Kitazawa, H. Takayanagi, J.M. Penninger, et al. 2008. The tumor necrosis factor family receptors RANK and CD40 cooperatively establish the thymic medullary microenvironment and self-tolerance. *Immunity.* 29:423–437. https://doi.org/10.1016/j.immuni.2008.06.015

Aliahmad, P., B. de la Torre, and J. Kaye. 2010. Shared dependence on the DNA-binding factor TOX for the development of lymphoid tissue-inducer cell and NK cell lineages. *Nat. Immunol.* 11:945–952. https://doi.org/10.1038/ni.1930

Bajoghli, B., N. Aghaallaei, I. Hess, I. Rode, N. Netuschil, B.H. Tay, B. Venkatesh, J.K. Yu, S.L. Kaltenbach, N.D. Holland, et al. 2009. Evolution of genetic networks underlying the emergence of thymopoiesis in vertebrates. *Cell.* 138:186–197. https://doi.org/10.1016/j.cell.2009.04.017

Baker, C.R., L.N. Booth, T.R. Sorrells, and A.D. Johnson. 2012. Protein modularity, cooperative binding, and hybrid regulatory states underlie transcriptional network diversification. *Cell.* 151:80–95. https://doi.org/10.1016/j.cell.2012.08.018

Boehm, T., and C.C. Bleul. 2006. Thymus-homing precursors and the thymic microenvironment. *Trends Immunol.* 27:477–484. https://doi.org/10.1016/j.it.2006.08.004

Boehm, T., S. Scheu, K. Pfeffer, and C.C. Bleul. 2003. Thymic medullary epithelial cell differentiation, thymocyte emigration, and the control of autoimmunity require lympho-epithelial cross talk via LTbetaR. *J. Exp. Med.* 198:757–769. https://doi.org/10.1084/jem.20030794

Boehm, T., I. Hess, and J.B. Swann. 2012. Evolution of lymphoid tissues. *Trends Immunol.* 33:315–321. https://doi.org/10.1016/j.it.2012.02.005

Braun, T., and A. Woollard. 2009. RUNX factors in development: Lessons from invertebrate model systems. *Blood Cells Mol. Dis.* 43:43–48. https://doi.org/10.1016/j.bcmd.2009.05.001

Calderón, L., and T. Boehm. 2011. Three chemokine receptors cooperatively regulate homing of hematopoietic progenitors to the embryonic mouse thymus. *Proc. Natl. Acad. Sci. USA.* 108:7517–7522. https://doi.org/10.1073/pnas.1016428108

de Bruijn, M.F., and N.A. Speck. 2004. Core-binding factors in hematopoiesis and immune function. *Oncogene.* 23:4238–4248. https://doi.org/10.1038/sj.onc.1207763

Donskoy, E., and I. Goldschneider. 1992. Thymocytopoiesis is maintained by blood-borne precursors throughout postnatal life. A study in parabiotic mice. *J. Immunol.* 148:1604–1612.

Eberl, G., S. Marmon, M.J. Sunshine, P.D. Rennert, Y. Choi, and D.R. Littman. 2004. An essential function for the nuclear receptor RORgamma(t) in the generation of fetal lymphoid tissue inducer cells. *Nat. Immunol.* 5:64–73. https://doi.org/10.1038/ni1022

Ebihara, T., C. Song, S.H. Ryu, B. Plougastel-Douglas, L. Yang, D. Levanon, Y. Groner, M.D. Bern, T.S. Stappenbeck, M. Colonna, et al. 2015. Runx3 specifies lineage commitment of innate lymphoid cells. *Nat. Immunol.* 16:1124–1133. https://doi.org/10.1038/ni.3272

Golling, G., L. Li, M. Pepling, M. Stebbins, and J.P. Gergen. 1996. Drosophila homologs of the proto-oncogene product PEBP2/CBF beta regulate the DNA-binding properties of Runt. *Mol. Cell. Biol.* 16:932–942. https://doi.org/10.1128/MCB.16.3.932

Gu, T.L., T.L. Goetz, B.J. Graves, and N.A. Speck. 2000. Auto-inhibition and partner proteins, core-binding factor beta (CBFbeta) and Ets-1, modulate DNA binding by CBFalpha2 (AML1). *Mol. Cell. Biol.* 20:91–103. https://doi.org/10.1128/MCB.20.1.91-103.2000

Hernández-Munain, C., and M.S. Krangel. 2002. Distinct roles for c-Myb and core binding factor/polyoma enhancer-binding protein 2 in the assembly and function of a multiprotein complex on the TCR delta enhancer in vivo. *J. Immunol.* 169:4362–4369. https://doi.org/10.4049/jimmunol.169.8.4362

Hess, I., and T. Boehm. 2012. Intravital imaging of thymopoiesis reveals dynamic lympho-epithelial interactions. *Immunity.* 36:298–309. https://doi.org/10.1016/j.immuni.2011.12.016

Jenkinson, W.E., S.W. Rossi, S.M. Parnell, W.W. Agace, Y. Takahama, E.J. Jenkinson, and G. Anderson. 2007. Chemokine receptor expression defines heterogeneity in the earliest thymic migrants. *Eur. J. Immunol.* 37:2090–2096. https://doi.org/10.1002/eji.200737212

Jiang, Q., X. Qin, T. Kawane, H. Komori, Y. Matsuo, I. Taniuchi, K. Ito, S. Izumi, and T. Komori. 2016. Cbfb2 isoform dominates more potent Cbfb1 and is required for skeletal development. *J. Bone Miner. Res.* 31:1391–1404. https://doi.org/10.1002/jbmr.2814

Kim, D., G. Pertea, C. Trapnell, H. Pimentel, R. Kelley, and S.L. Salzberg. 2013. TopHat2: Accurate alignment of transcriptomes in the presence of insertions, deletions and gene fusions. *Genome Biol.* 14:R36. https://doi.org/10.1186/gb-2013-14-4-r36

Kim, W.Y., M. Sieweke, E. Ogawa, H.J. Wee, U. Englmeier, T. Graf, and Y. Ito. 1999. Mutual activation of Ets-1 and AML1 DNA binding by direct interaction of their autoinhibitory domains. *EMBO J.* 18:1609–1620. https://doi.org/10.1093/emboj/18.6.1609

Kivioja, T., A. Vähärautio, K. Karlsson, M. Bonke, M. Enge, S. Linnarsson, and J. Taipale. 2012. Counting absolute numbers of molecules using unique molecular identifiers. *Nat. Methods.* 9:72–74. https://doi.org/10.1038/nmeth.1778

Krangel, M.S. 2009. Mechanics of T cell receptor gene rearrangement. *Curr. Opin. Immunol.* 21:133–139. https://doi.org/10.1016/j.coi.2009.03.009

Krishnamoorthy, V., T. Carr, R.F. de Pooter, A.O. Emanuelle, F. Gounari, and B.L. Kee. 2015. Repression of Ccr9 transcription in mouse T lymphocyte progenitors by the Notch signaling pathway. *J. Immunol.* 194:3191–3200. https://doi.org/10.4049/jimmunol.1402443

Krueger, A., S. Willenzon, M. Lyszkiewicz, E. Kremmer, and R. Förster. 2010. CC chemokine receptor 7 and 9 double-deficient hematopoietic progenitors are severely impaired in seeding the adult thymus. *Blood.* 115:1906–1912. https://doi.org/10.1182/blood-2009-07-235721

Lam, S.H., H.L. Chua, Z. Gong, T.J. Lam, and Y.M. Sin. 2004. Development and maturation of the immune system in zebrafish, Danio rerio: A gene expression profiling, in situ hybridization and immunological study. *Dev. Comp. Immunol.* 28:9–28. https://doi.org/10.1016/S0145-305X(03)00103-4

Liu, C., F. Saito, Z. Liu, Y. Lei, S. Uehara, P. Love, M. Lipp, S. Kondo, N. Manley, and Y. Takahama. 2006. Coordination between CCR7- and CCR9-mediated chemokine signals in prevascular fetal thymus colonization. *Blood.* 108:2531–2539. https://doi.org/10.1182/blood-2006-05-024190

Masuda, K., H. Kubagawa, T. Ikawa, C.C. Chen, K. Kakugawa, M. Hattori, R. Kageyama, M.D. Cooper, N. Minato, Y. Katsura, and H. Kawamoto. 2005. Prethymic T-cell development defined by the expression of paired immunoglobulin-like receptors. *EMBO J.* 24:4052–4060. https://doi.org/10.1038/sj.emboj.7600878

Mebius, R.E. 2003. Organogenesis of lymphoid tissues. *Nat. Rev. Immunol.* 3:292–303. https://doi.org/10.1038/nri1054

Mebius, R.E., P.R. Streeter, S. Michie, E.C. Butcher, and I.L. Weissman. 1996. A developmental switch in lymphocyte homing receptor and endothelial vascular addressin expression regulates lymphocyte homing and permits CD4+ CD3- cells to colonize lymph nodes. *Proc. Natl. Acad. Sci. USA.* 93:11019–11024. https://doi.org/10.1073/pnas.93.20.11019

Nah, G.S., Z.W. Lim, B.H. Tay, M. Osato, and B. Venkatesh. 2014a. Runx family genes in a cartilaginous fish, the elephant shark (Callorhinchus milii). *PLoS One.* 9:e93816. https://doi.org/10.1371/journal.pone.0093816

Nah, G.S., B.H. Tay, S. Brenner, M. Osato, and B. Venkatesh. 2014b. Characterization of the Runx gene family in a jawless vertebrate, the Japanese lamprey (Lethenteron japonicum). *PLoS One.* 9:e113445. https://doi.org/10.1371/journal.pone.0113445

Naoe, Y., R. Setoguchi, K. Akiyama, S. Muroi, M. Kuroda, F. Hatam, D.R. Littman, and I. Taniuchi. 2007. Repression of interleukin-4 in T helper type 1 cells by Runx/Cbf β binding to the Il4 silencer. *J. Exp. Med.* 204:1749–1755. https://doi.org/10.1084/jem.20062456

Ng, C.E., M. Osato, B.H. Tay, B. Venkatesh, and Y. Ito. 2007. cDNA cloning of Runx family genes from the pufferfish (Fugu rubripes). *Gene.* 399:162–173. https://doi.org/10.1016/j.gene.2007.05.014

Ogawa, E., M. Inuzuka, M. Maruyama, M. Satake, M. Naito-Fujimoto, Y. Ito, and K. Shigesada. 1993. Molecular cloning and characterization of PEBP2 beta, the heterodimeric partner of a novel Drosophila runt-related DNA binding protein PEBP2 alpha. *Virology.* 194:314–331. https://doi.org/10.1006/viro.1993.1262

Ogawa, T., K. Kryukov, T. Imanishi, and K. Shiroguchi. 2017. The efficacy and further functional advantages of random-base molecular barcodes for absolute and digital quantification of nucleic acid molecules. *Sci. Rep.* 7:13576. https://doi.org/10.1038/s41598-017-13529-329051542

Owen, J.J., and M.A. Ritter. 1969. Tissue interaction in the development of thymus lymphocytes. *J. Exp. Med.* 129:431–442. https://doi.org/10.1084/jem.129.2.431

Payer, E., A. Elbe, and G. Stingl. 1991. Circulating CD3+/T cell receptor V gamma 3+ fetal murine thymocytes home to the skin and give rise to proliferating dendritic epidermal T cells. *J. Immunol.* 146:2536–2543.

Sakuma, T., Q.L. Li, Y. Jin, L.B. Choi, E.G. Kim, K. Ito, Y. Ito, S. Nomura, and S.C. Bae. 2001. Cloning and expression pattern of a novel PEBP2 beta-binding protein (charged amino acid rich leucine zipper-1[Crl-1]) in the mouse. *Mech. Dev.* 104:151–154. https://doi.org/10.1016/S0925-4773(01)00366-5

Shiroguchi, K., T.Z. Jia, P.A. Sims, and X.S. Xie. 2012. Digital RNA sequencing minimizes sequence-dependent bias and amplification noise with optimized single-molecule barcodes. *Proc. Natl. Acad. Sci. USA.* 109:1347–1352. https://doi.org/10.1073/pnas.1118018109

Sun, Z., D. Unutmaz, Y.R. Zou, M.J. Sunshine, A. Pierani, S. Brenner-Morton, R.E. Mebius, and D.R. Littman. 2000. Requirement for RORgamma in thymocyte survival and lymphoid organ development. *Science.* 288:2369–2373. https://doi.org/10.1126/science.288.5475.2369

Tachibana, M., M. Tenno, C. Tezuka, M. Sugiyama, H. Yoshida, and I. Taniuchi. 2011. Runx1/Cbfβ2 complexes are required for lymphoid tissue inducer cell differentiation at two developmental stages. *J. Immunol.* 186:1450–1457. https://doi.org/10.4049/jimmunol.1000162

Taniuchi, I., M. Osato, T. Egawa, M.J. Sunshine, S.C. Bae, T. Komori, Y. Ito, and D.R. Littman. 2002. Differential requirements for Runx proteins in CD4 repression and epigenetic silencing during T lymphocyte development. *Cell.* 111:621–633. https://doi.org/10.1016/S0092-8674(02)01111-X

Teichmann, S.A., and M.M. Babu. 2004. Gene regulatory network growth by duplication. *Nat. Genet.* 36:492–496. https://doi.org/10.1038/ng1340

Tenno, M., K. Shiroguchi, S. Muroi, E. Kawakami, K. Koseki, K. Kryukov, T. Imanishi, F. Ginhoux, and I. Taniuchi. 2017. Cbfβ2 deficiency preserves Langerhans cell precursors by lack of selective TGFβ receptor signaling. *J. Exp. Med.* 214:2933–2946. https://doi.org/10.1084/jem.20170729

Uehara, S., A. Grinberg, J.M. Farber, and P.E. Love. 2002. A role for CCR9 in T lymphocyte development and migration. *J. Immunol.* 168:2811–2819. https://doi.org/10.4049/jimmunol.168.6.2811

Wang, Q., T. Stacy, J.D. Miller, A.F. Lewis, T.L. Gu, X. Huang, J.H. Bushweller, J.C. Bories, F.W. Alt, G. Ryan, et al. 1996. The CBFbeta subunit is essential for CBFalpha2 (AML1) function in vivo. *Cell.* 87:697–708. https://doi.org/10.1016/S0092-8674(00)81389-6

Wang, S., Q. Wang, B.E. Crute, I.N. Melnikova, S.R. Keller, and N.A. Speck. 1993. Cloning and characterization of subunits of the T-cell receptor and murine leukemia virus enhancer core-binding factor. *Mol. Cell. Biol.* 13:3324–3339. https://doi.org/10.1128/MCB.13.6.3324

Woolf, E., O. Brenner, D. Goldenberg, D. Levanon, and Y. Groner. 2007. Runx3 regulates dendritic epidermal T cell development. *Dev. Biol.* 303:703–714. https://doi.org/10.1016/j.ydbio.2006.12.005

Yang, Q., J. Jeremiah Bell, and A. Bhandoola. 2010. T-cell lineage determination. *Immunol. Rev.* 238:12–22. https://doi.org/10.1111/j.1600-065X.2010.00956.x

Yui, M.A., and E.V. Rothenberg. 2014. Developmental gene networks: A triathlon on the course to T cell identity. *Nat. Rev. Immunol.* 14:529–545. https://doi.org/10.1038/nri3702

Zaiman, A.L., A.F. Lewis, B.E. Crute, N.A. Speck, and J. Lenz. 1995. Transcriptional activity of core binding factor-alpha (AML1) and beta subunits on murine leukemia virus enhancer cores. *J. Virol.* 69:2898–2906.

Zetsche, B., J.S. Gootenberg, O.O. Abudayyeh, I.M. Slaymaker, K.S. Makarova, P. Essletzbichler, S.E. Volz, J. Joung, J. van der Oost, A. Regev, et al. 2015. Cpf1 is a single RNA-guided endonuclease of a class 2 CRISPR-Cas system. *Cell.* 163:759–771. https://doi.org/10.1016/j.cell.2015.09.038

Zhang, S.L., and A. Bhandoola. 2014. Trafficking to the thymus. *Curr. Top. Microbiol. Immunol.* 373:87–111.

Zlotoff, D.A., A. Sambandam, T.D. Logan, J.J. Bell, B.A. Schwarz, and A. Bhandoola. 2010. CCR7 and CCR9 together recruit hematopoietic progenitors to the adult thymus. *Blood.* 115:1897–1905. https://doi.org/10.1182/blood-2009-08-237784